Draft version May 12, 2020
Typeset using LaTeX default style in AASTeX63

Galaxy And Mass Assembly: A Comparison between Galaxy-Galaxy Lens Searches in KiDS/GAMA.

Shawn Knabel,[1] Rebecca L. Steele,[1] Benne W. Holwerda,[1] Joanna S. Bridge,[1] Alice Jacques,[1] Andrew M. Hopkins,[2] Stephen P. Bamford,[3] Michael J. I. Brown,[4] Sarah Brough,[5] Lee Kelvin,[6] and Maciej Bilicki[7]

[1] *Department of Physics and Astronomy, 102 Natural Science Building, University of Louisville, Louisville KY 40292, USA*
[2] *Australian Astronomical Optics, Macquarie University, 105 Delhi Rd, North Ryde, NSW 2113, Australia*
[3] *School of Physics & Astronomy, University of Nottingham, University Park, Nottingham, NG7 2RD, UK*
[4] *School of Physics & Astronomy, Monash University, Clayton, VIC 3800, Australia*
[5] *School of Physics, University of New South Wales, NSW 2052, Australia*
[6] *Department of Astrophysical Sciences, Princeton University, 4 Ivy Lane, Princeton, NJ 08544, USA*
[7] *Center for Theoretical Physics, Polish Academy of Sciences, Warsaw, Poland*

Submitted to AJ

ABSTRACT

Strong gravitational lenses are a rare and instructive type of astronomical object. Identification has long relied on serendipity, but different strategies – such as mixed spectroscopy of multiple galaxies along the line of sight, machine learning algorithms, and citizen science – have been employed to identify these objects as new imaging surveys become available.

We report on the comparison between spectroscopic, machine learning, and citizen science identification of galaxy-galaxy lens candidates from independently constructed lens catalogs in the common survey area of the equatorial fields of the Galaxy and Mass Assembly (GAMA) survey. In these, we have the opportunity to compare high-completeness spectroscopic identifications against high-fidelity imaging from the Kilo Degree Survey (KiDS) used for both machine learning and citizen science lens searches.

We find that the three methods – spectroscopy, machine learning, and citizen science – identify 47, 47 and 36 candidates respectively in the 180 square degrees surveyed. These identifications barely overlap, with only two identified by both citizen science and machine learning. We have traced this discrepancy to inherent differences in the selection functions of each of the three methods, either within their parent samples (i.e. citizen science focuses on low-redshift) or inherent to the method (i.e. machine learning is limited by its training sample and prefers well-separated features, while spectroscopy requires sufficient flux from lensed features to lie within the fiber). These differences manifest as separate samples in estimated Einstein radius, lens stellar mass, and lens redshift. The combined sample implies a sky-density of ~ 0.72 deg^{-2} and can inform the construction of a training set spanning a wider mass-redshift space. A combined approach and refinement of automated searches would result in a more complete sample of galaxy-galaxy lenses for future surveys.

Keywords: Strong gravitational lensing, Galaxy dark matter halos, Redshift surveys, Giant elliptical galaxies

1. INTRODUCTION

Elliptical galaxies' structure, kinematics, and formation histories are a compelling test of the Cold Dark Matter (ΛCDM) paradigm as they are the end-product of galaxy formation (De Lucia et al. 2006). Strong gravitational lenses appear in every respect to be just like other elliptical galaxies, so results of their study can therefore be generalized to all spheroidal galaxies in the observed mass range (Auger et al. 2009a). These lensing systems provide a highly accurate measurement of the *total* mass, and therefore the dark matter content, in these elliptical galaxies that compares well with current galaxy evolution models and assumptions (Shu et al. 2014, and reference therein). To date, gravitational

lenses have proven General Relativity to be correct with high accuracy over galaxy-wide scales (Collett et al. 2018) and may provide an excellent test case for other theories of gravity, such as the Emergent Gravity recently proposed by Verlinde (2016), through a combination of lensing and kinematic measurements (see Tortora et al. 2017).

Gravitational lensing has been a powerful technique to measure the masses of the *most massive* elliptical galaxies (Gavazzi et al. 2007; **?**), constraining their Fundamental Plane (Bolton et al. 2008b), the stellar population's mass-to-light ratio, and thus their initial mass function (IMF; Auger et al. 2009a; Hopkins 2018). The observational drive is now to measure their mass content throughout the spheroidal galaxy mass function (Bolton et al. 2006; **?**), explore the Fundamental Plane in different environments (Treu et al. 2009), constrain the stellar mass-to-light ratio in nearby ellipticals (Treu et al. 2006; Collier et al. 2018a,b), discover dark matter substructure in known strong galaxy lens cases (Cyr-Racine et al. 2018), and independently measure H_0 through time-delay cosmography (e.g. H0LiCOW, Chen et al. 2019). These observational studies need larger samples of lenses.

Thus far, lensing arcs have predominantly been identified in *massive* ($> 10^{11} M_{\odot}$) lens systems thanks to selection biases: SDSS spectroscopic targets are volume-weighted to greater mass, and visual identification favors well-separated arc and lens (Shu et al. 2014). With the GAMA spectroscopy-selected sample (Holwerda et al. 2015), a much greater range in lens masses is now available. However, the drive for much larger samples has led to increased searches using machine learning to constrain ΛCDM in detail (Petrillo et al. 2017, 2018; **?**; Speagle et al. 2019; Huang et al. 2019; Jacobs et al. 2019; Li et al. 2020).

The success and completeness of the different identification techniques are difficult to test against one another. This has motivated our study here that benefits from three independent identifications – spectroscopic, machine learning and citizen science – on the same target fields. Our aim is to compare all three techniques to map out an optimal path for future searches.

2. IDENTIFYING STRONG GALAXY-GALAXY LENSES

The principal selection technique for galaxy-galaxy lenses has been the identification of double spectral profiles in a single aperture based spectrum (blended spectra, see Bolton et al. 2004; Holwerda et al. 2015, Steele et al. *in prep.*). Searches for blended spectra in the Sloan Digital Sky Survey (SDSS) have been highly successful in identifying strong-lens candidate galaxies by identifying spectra containing both a low-redshift passive galaxy and emission lines from a much higher-redshift lensed source. In order to confirm such sources as true lensing systems, one requires significantly higher spatial resolution imaging than SDSS can provide.

85 cases of strong lenses have already been confirmed with Hubble Space Telescope (HST) imaging through the SLACS (Sloan Lens ACS) survey (Treu et al. 2006; Koopmans et al. 2006; Gavazzi et al. 2007; **?**, 2008; Bolton et al. 2008b; Treu et al. 2009; Auger et al. 2009a). The SLACS survey was efficient in finding these rare strong lensing objects: approximately 50% of the blended spectra (with a dispersion estimate of the Einstein radius) targeted were confirmed with HST observations, and its success has expanded into the BOSS survey and higher redshifts ($0.4 < z < 0.7$, Brownstein et al. 2012).

However, due to the depth and completeness limitations of SDSS spectroscopy – main survey depth is $m_r < 17.7$; LRG sample leads to effective constraints on redshift to $m_r < 19.5$ (Eisenstein et al. 2001) – typically only massive foreground galaxy lenses can be identified ($10^{11} - 10^{12} M_{\odot}$) at intermediate redshifts ($z = 0.15 - 1$). In addition, the SLACS survey (SLACS & S4TM, Shu et al. 2015) imposed a redshift cut of z > 0.15 for the majority of the lens candidates that were selected from the LRG sample. According to Hilbert et al. (2008) the lensing cross section drops rapidly below $z \sim 0.5$, so naturally there are fewer lenses at lower redshifts. However, Sonnenfeld et al. (2015), referencing Arneson et al. (2012) and **?**, points to the Einstein radius as the main quantity determining the detection probability as opposed to the lensing cross-section. Einstein radius is a function of the mass and redshift arrangement, with higher mass and closer lenses resulting in larger Einstein radii. Lens candidate identification through any spectroscopic method requires sufficient flux from the background galaxy in order to obtain a second spectral match. For lensing systems whose Einstein radius exceeds the radius of the instruments aperture (1.5″-radius for SDSS), the probability of detection goes down significantly (Sonnenfeld et al. 2015, and reference therein). Only with a significant expansion of the lensing sample can the effects of evolution and stellar mass be decoupled (e.g., Treu et al. 2006). In the following calculations we adopt a cosmological model with $h_0 = 0.738$, where $h_0 = \frac{H_0}{100}$ $kms^{-1}Mpc^{-1}$ indicated in Riess et al. (2011).

2.1. *GAMA Spectroscopic Identification*

The Galaxy and Mass Assembly survey (GAMA; Driver et al. 2009, 2011) is a multi-wavelength survey built around a deep and highly complete redshift survey of five fields with the Anglo-Australian Telescope. GAMA has three major advantages over SDSS in the identification of blended spectra: (1) the spectroscopic limiting depth is 2 magnitudes deeper ($m_r < 19.8$ mag.), (2) the completeness is close to 98% (Liske et al. 2015), and (3) the AUTOZ redshift algorithm easily identifies spectra with signal from two different redshifts (Baldry et al. 2014). In the GAMA survey, Holwerda et al. (2015) identified 104 strong lensing candidates from their blended spectra. Chan et al. (2016) verified 10 of a subset of 14 of these spectroscopically identified lenses using deep Subaru imaging. This GAMA spectroscopy sample is dominated by lower-mass spheroidal galaxies and higher-redshift galaxies (Steele et al. *in prep.*). These GAMA strong lens candidates from (Holwerda et al. 2015, Steele et al. *in prep.*) extend the stellar mass range and provide a medium-redshift observation in between the SLACS, S4TM, and BELLS samples.

As mentioned above, the spectroscopic approach is intrinsically limited by the aperture of the spectroscopy: if the lensed features fall outside it, the signal of the lensed (source) galaxy will be weak and unlikely to be detected (Sonnenfeld et al. 2015, and reference therein). As a result of this, GAMA spectroscopy's 1″-radius aperture structurally misses lower redshift and higher mass lens candidates. GAMA has improved the spectroscopic identification of lower mass strong lenses, but a much larger sample of lower redshift ($z < 0.1$) lenses is needed to constrain mass-to-light ratios in ellipticals.

2.2. *Beyond Spectroscopic Identification of Lenses*

2.2.1. *Machine Learning Identification of Lenses*

Machine learning is gaining popularity as a method for identifying galaxy-galaxy lens candidates, e.g. in Subaru Hyper-Supreme Cam (Speagle et al. 2019), DECAM (Huang et al. 2019), and Dark Energy Survey data (Jacobs et al. 2019). Petrillo et al. (2017) and Petrillo et al. (2018) introduced and developed a machine learning technique to visually identify strong lens candidates by training the neural networks to recognize the characteristic arcs that appear next to a lensing elliptical galaxy using simulated images resembling SLACS lenses as their training set. Their selection process included a follow-up visual inspection of each candidate by seven members of the team, which provided a score for each candidate between 0 (reflecting low confidence) and 70 (reflecting high confidence). This new identification method resulted in the ∼1300 candidate galaxy-galaxy lenses in the Kilo-Degree Survey (LinKS) sample (KiDS; de Jong et al. 2013, 2015, 2017; Kuijken et al. 2019), which overlaps with 100% of the equatorial fields of the GAMA survey (fields G09, G12, and G15). These identifications by Petrillo et al. (2018) have shown that there are many more strong lenses to be found in the same survey area using identification methods other than spectroscopic. This approach has succeeded in finding more candidate strong lenses similar to the simulated massive elliptical galaxies on which the neural network was trained, ie. large ellipticals with characteristics similar to those of SLACS lens candidates.

2.2.2. *Citizen Science Identification of Lenses*

GalaxyZoo (Lintott et al. 2008) has classified KiDS postage stamps of galaxies on the same area that corresponds to the GAMA+KiDS survey overlap (Kelvin et al. *in prep*, Holwerda et al. 2019) using a question tree design shown below in Figure 1. It leads participants through a series of questions that (given the object is a galaxy) will arrive at a question that prompts them to identify any number of the following "odd features" in the image: "None", "Ring", "Lens or arc", "Dust lane", "Irregular", "Other", and "Overlapping". With the voting completed on the GAMA+KiDS equatorial fields, we can now analyze the results of the citizen science approach.

With three independent techniques to identify strong gravitational lenses in the same three fields, we have an opportunity to test how well different identification techniques can be calibrated against one another, discover implicit selection effects in each, and approximate the on-sky density of strong galaxy lenses.

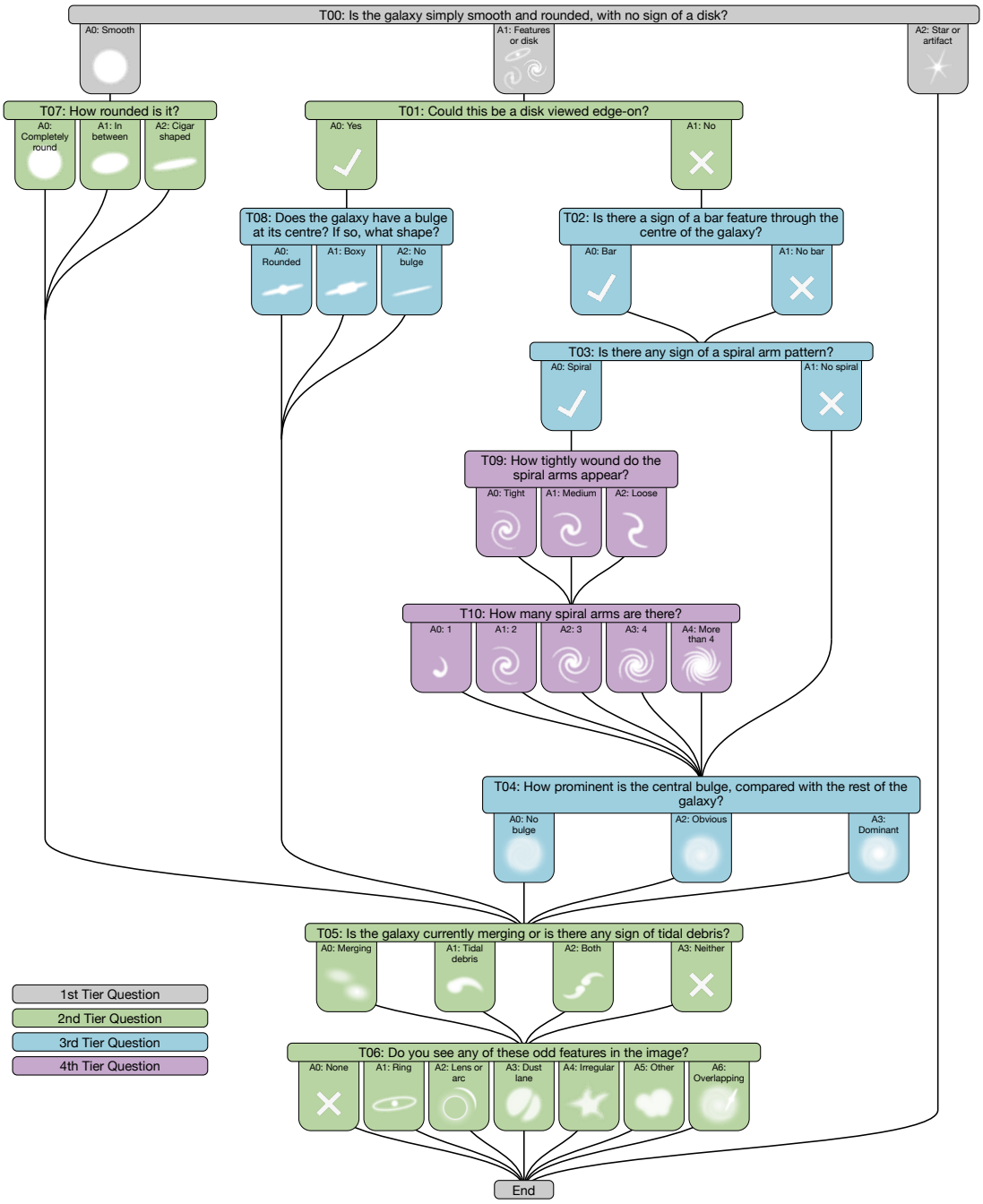

Figure 1. The question tree employed by GalaxyZoo citizen science, which volunteer participants use to classify images from the Kilo-Degree Survey (KiDS). 2nd Tier Question T06 prompts participants to identify "odd features," of which an option is "Lens or arc." Participants can choose more than one option in T06. We used results from this question to determine the final cut for our GalaxyZoo selection.

3. DATA AND OBSERVATIONS

In order to obtain a valid comparison of the three techniques, the catalogs of candidate lenses obtained by GAMA blended spectra (Holwerda et al. 2015), LinKS machine learning (Petrillo et al. 2018), and GalaxyZoo citizen science (Kelvin et al. *in prep.*) were cut to represent only those candidates identified within the equatorial GAMA fields G09, G12, and G15, which is the area of overlap between GAMA and KiDS. We show the presence of candidates identified by each method in each of those fields in Figure 2. This cut resulted in usable catalogs consisting of 85 spectroscopically-identified lens candidates, 421 candidates identified by LinKS machine learning, and a misleading total of 12934 GalaxyZoo candidates with "Lens or arc" scores of 0 or higher. Further cuts (see below in Sections 3.1 and 3.2) to the catalogs were then made to account for false positives in each of the samples.

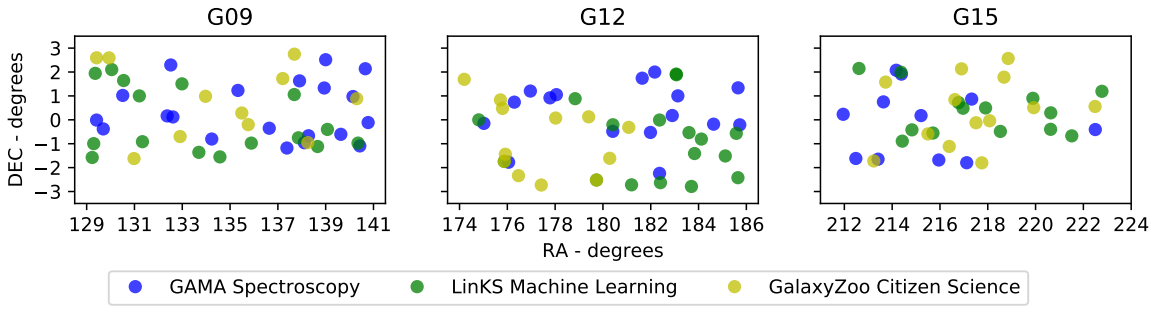

Figure 2. The three GAMA/KiDS fields (G09, G12 and G15) within which all three lensing identification techniques are available. GAMA spectroscopic, LinKS machine learning, and GalaxyZoo citizen science and identifications of galaxy-galaxy lens candidate systems are identified in all three fields.

Stellar mass estimates and redshifts for each candidate were taken from the GAMA MAGPHYS catalog (Wright et al. 2018) and checked with WISE masses (Cluver et al. 2014) from GAMA DR2/3 (Liske et al. 2015; Baldry et al. 2018). Candidates were matched between independent catalogs by GAMA ID, except for the LinKS sample, which was matched based on RA and DEC.

3.1. *GAMA Blended Spectra and LinKS Machine Learning Catalogs*

The lens candidate sample provided by Holwerda et al. (2015) is based on spectral match, and therefore does not include a subjective follow-up visual inspection. However, in order to attain a more pure sample for consideration here, we selected candidates with a minimum difference of $\Delta z > 0.1$ between the redshift of the passive galaxy spectral match and an emission line galaxy match at higher redshift. This selection is shown in Figure 3 in comparison to Grade-A SLACS lenses from Auger et al. (2009b). Note that first redshift matches for GAMA spectroscopy do not necessarily correspond to the closer of the two galaxies. In all cases, the closer of the two is the passive galaxy, even if the first spectral match was to the emission line galaxy. The result of this selection is 47 candidates identified by GAMA spectroscopy.

The LinKS machine learning catalog of 421 candidates obtained from Petrillo et al. (2018) included all those objects whose visual inspection score was greater than 0. In order to compare only the highest quality candidates, a score threshold of > 17 was taken from Petrillo et al. (2017). This reduced the LinKS machine learning catalog to 47. All following mentions of the GAMA spectroscopy and LinKS machine learning samples refer to these reduced selections of candidates unless otherwise specified.

3.2. *Citizen Science (GalaxyZoo) catalog*

GalaxyZoo presented the most variables to consider when analyzing its reliability as a method for identifying strong lenses. The percentage of votes for lensing features in each candidate is taken to be a subjective score given in a similar manner to the LinKS machine learning catalog. Since the program was not designed specifically to identify

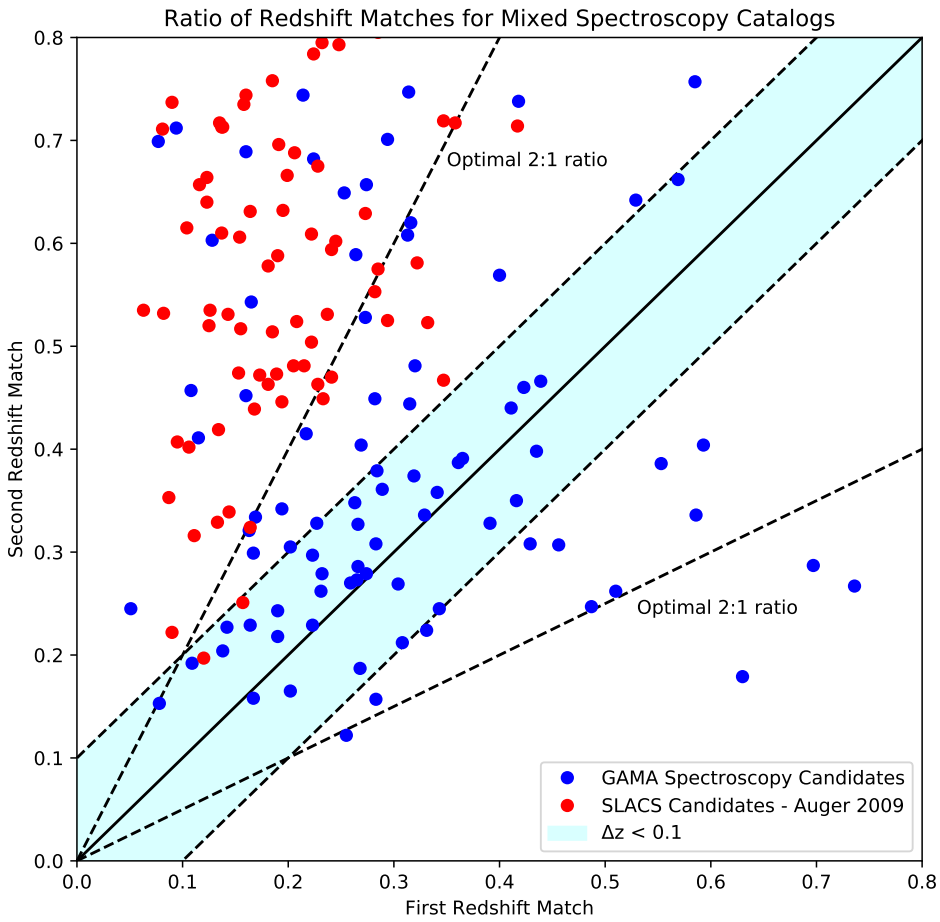

Figure 3. Selection of GAMA spectroscopy candidates based on redshift difference between lens and source. Blue markers denote GAMA spectroscopy candidates from Holwerda et al. (2015). In all cases, the passive galaxy match is at lower redshift than the emission line galaxy match. The shaded area represents redshift differences of less than 0.1, which indicate unlikely lens candidates. We remove all GAMA spectroscopy candidates within this shaded region. Red markers show redshift difference for SLACS candidates taken from Auger et al. (2009b).

only lenses, each candidate's score must also be considered relative to scores of other choices within the same question level. For each candidate in question, other "odd features" could potentially pull votes away from the "Lens or arc" classification.

Selection votes could be distributed unpredictably across the seven options, so we took a multi-faceted selection cutoff informed by visual comparison of candidates of a range of "Lens or arc" scores, examples of which are shown in Figure 4, as well as comparing them with LinKS machine learning candidates, in addition to analyzing ratios of "Lens or arc" scores to the scores given to each of the other six "odd feature" options, which we demonstrate in Figure 5. We considered doubt in the participants' visual inspection to bias the selection toward "None" if features did not seem "odd" enough, so we added an additional provision to our cutoff. Our final selection considered only those candidates with the following characteristics:

1. "Lens or Arc" score was greater than all other "odd feature" options' scores with the exception of "None".

2. "Lens or Arc" score was greater than half the score given to "None".

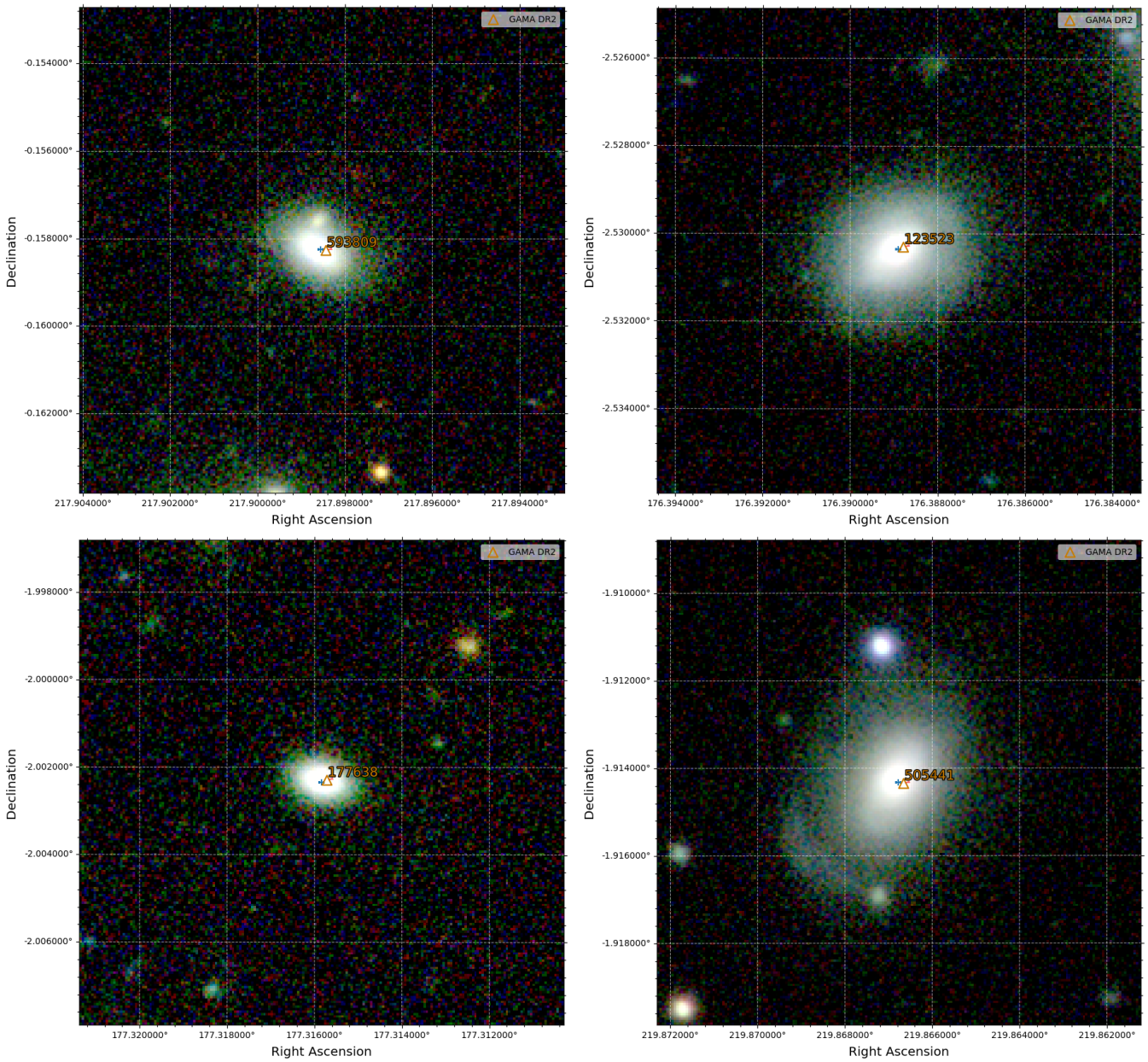

Figure 4. Examples of lens candidates identified by GalaxyZoo citizen science, taken from KiDS (*g-, r-,* and *i*-bands). G593809 (top left) represents a "Lens or arc" score of 10% of votes. G123523 (top right) represents a "Lens or arc" score of 20%. G177638 (bottom left) represents a "Lens or arc" score of 25%. G505441 (bottom right) represents a "Lens or arc" score of 30%. These are representative of the images that would be viewed by GalaxyZoo participants, as well as informing our final cutoff for the GalaxyZoo selection considered here.

3. "Lens or Arc" score was greater than 30 percent.

In addition, only those candidates whose estimated Einstein radius (Section 3.3 for details) is larger than the point spread function (PSF) for KiDS imaging (0.65 arcsec) were included in the final selection. This selection, based on the capabilities of the instrument, removes several high-scoring candidates from consideration, as shown in Figure 6. These removed objects are worth follow-up as candidates for galaxies showing tidal features.

This final cut reduced the GalaxyZoo citizen science catalog to 36 candidates (listed in Table 3 in the Appendix) of roughly comparable reliability to the other two techniques, according to our own visual inspection of various scoring lens candidates. The GalaxyZoo team imposed a redshift restriction of $z < 0.15$ in the pre-selection of images to be

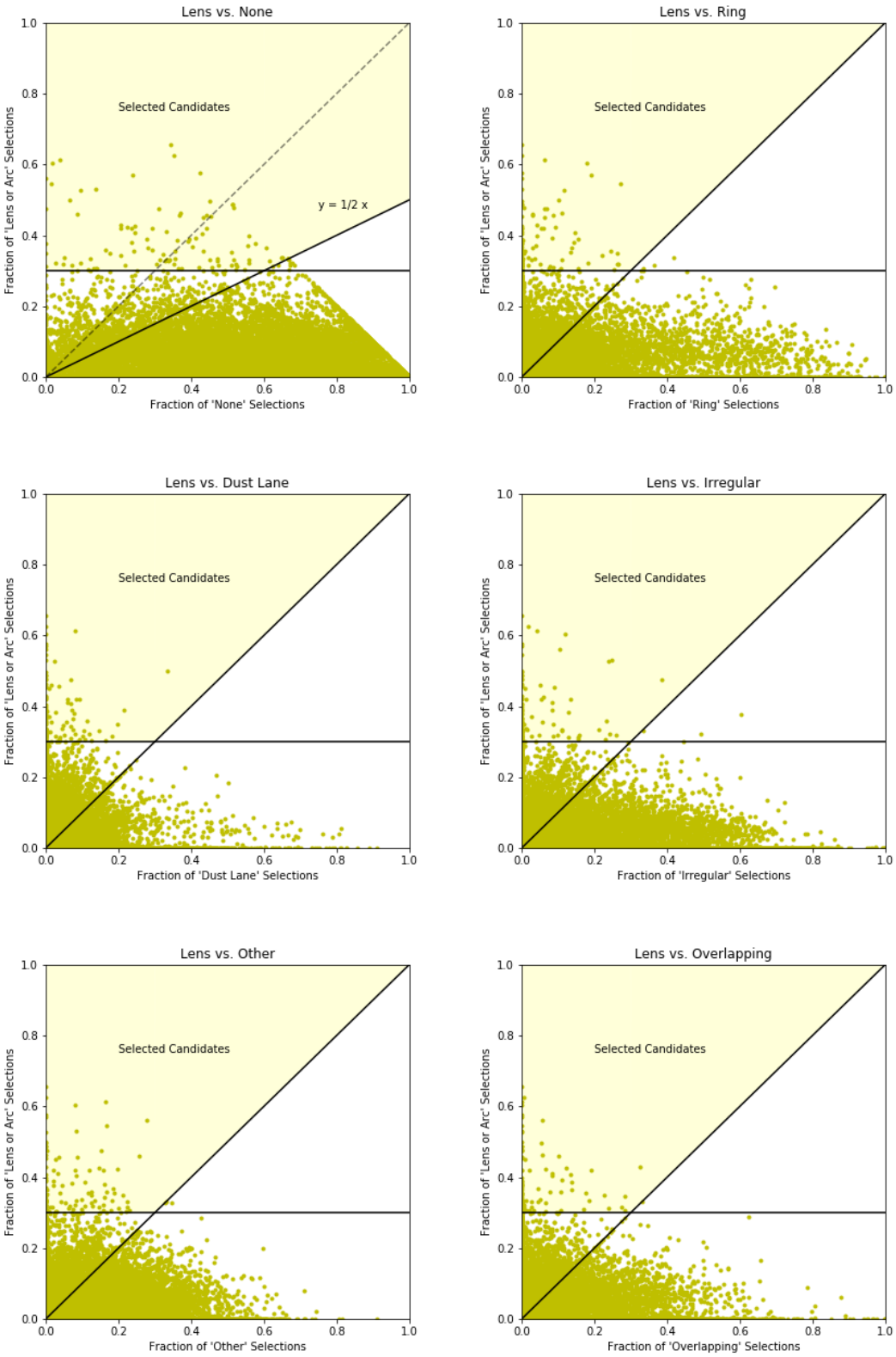

Figure 5. Ratios of the fractions of "Lens or arc" scores on the vertical axis with respect to the fractions of the other six "odd features" options from GalaxyZoo Question Tree question T06, shown above in Figure 1, scores on the horizontal axis. Solid lines indicate boundaries used in the final cut for the GalazyZoo selection. Only points that fall within the shaded region of all six plots are selected for our final GalaxyZoo sample.

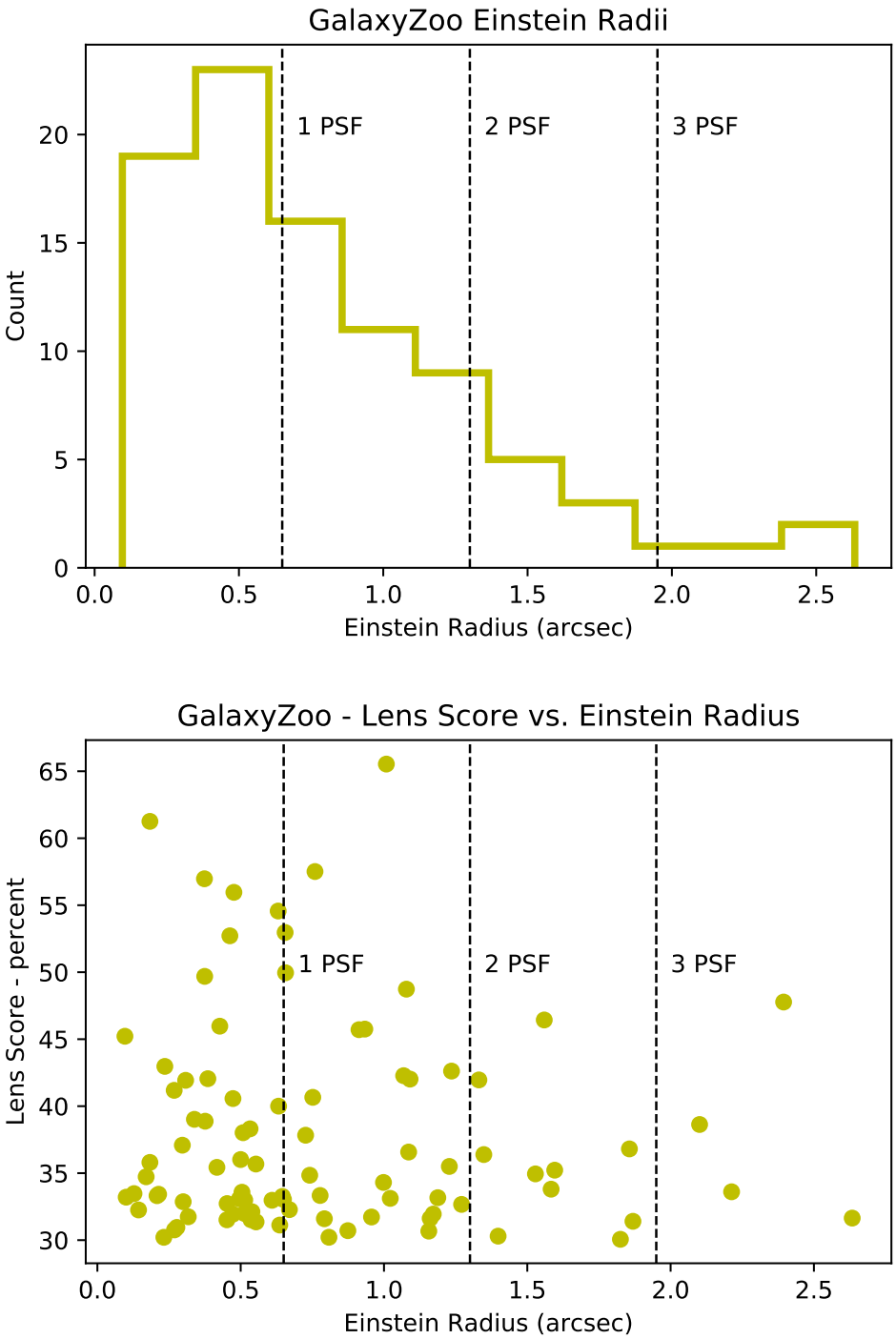

Figure 6. (Top) Histogram showing the distribution of Einstein radius estimates for GalaxyZoo citizen science candidates that pass the question tree portion of selection criteria. (Bottom) Vertical axis shows "Lens or arc" score as percentage of votes. Candidates with estimated Einstein radii lower than the KiDS PSF are considered poor candidates and are removed from the final sample. The high scoring GalaxyZoo objects in this removed subsample are good candidates for tidal features.

classified by participants. All following mentions of the GalaxyZoo citizen science sample refer to this reduced selection of candidates unless otherwise specified.

3.3. *Einstein Radius Estimation*

Limited by the exclusion of velocity dispersion measurements of the GAMA/KiDS fields, we approximate the lens galaxy as a point-mass system with the lens and source positioned along the same line of sight, where the Einstein radius (θ_E) is given by

$$\theta_E = (\frac{M}{10^{11.09} M_\odot})^{1/2} (\frac{D_{LS}}{D_L D_S} Mpc)^{1/2} arcsec$$

where M is the total mass enclosed by the Einstein radius, D_{LS} is the distance from lens to source, D_L is the distance from observer to lens, and D_S is the distance from observer to source. Utilizing stellar mass measurements from the GAMA MAGPHYS catalog (Wright et al. 2018) and assuming dark matter fraction of f_{DM} 61% (average taken from Barnabè et al. (2011) assuming Chabrier IMF), we estimate the total mass. Only the GAMA spectroscopy candidates include source redshift measurements; for these candidates, D_{LS} and D_S are calculated from this redshift. For LinKS machine learning and GalaxyZoo citizen science candidates, the lens galaxy is assumed to be positioned approximately halfway between the observer and source. This is the distance at which the most prominent features should be observable. Calculations performed here are considered to be underestimates due to the conservative assumption of an average f_{DM} that is in reality mass-weighted Barnabè et al. (2011) and likely higher for several candidates.

4. RESULTS

We found remarkably little overlap between catalogs of candidates obtained by the three methods. Our final cuts of the three catalogs included no candidate common to all three methods and only two candidates common to two methods, both of which were between LinKS machine learning and GalaxyZoo citizen science, as shown in Figure 7.

4.1. *Results of Einstein Radius Estimates*

The Einstein radius is a fundamental feature of a lensing system that determines to a large degree the probability of detection by any lens finding method (Sonnenfeld et al. 2015, and reference therein). The results of the estimates, displayed in the upper plot of Figure 8, show that the majority of GAMA spectroscopy candidates have Einstein radii smaller than or close to the 1″ GAMA spectroscopy aperture radius, as expected. The majority of candidates from the image-based machine learning and citizen science methods have characteristic Einstein radii close to or greater than 1 arcsecond, above the PSF where images of the lens galaxy and arc features can be distinctly separable. Reference θ_E estimates of SLACS (Bolton et al. 2008a) S4TM (Shu et al. 2017), and BELLS (Brownstein et al. 2012) grade-A lens candidates are shown in the lower plot of Figure 8. The LinKS machine learning sample identified candidates with comparable Einstein radii to the SLACS sample (which was the guide for its training sample), and S4TM and BELLS can be seen to approach the smaller Einstein radii identified in GAMA spectroscopy. GAMA spectroscopic candidates extend to lower Einstein radii than other spectroscopic selections because GAMA's high completeness reduces mass bias.

4.2. *Stellar Mass and Redshift Space*

Analyzing the properties of each catalog in terms of the candidates' stellar mass and redshift, which we illustrate in Figure 9, we discovered that each method identified galaxies within a distinct region of the parameter space.

The candidates identified through GAMA spectroscopy tended to be found between $z \sim 0.1 - 0.4$ and with stellar masses between $\log(M_*/M_\odot) \sim 10.5 - 11.25$, with a few below $\log(M_*/M_\odot)$ 10. For each redshift in the range, there is a maximum total mass for which the Einstein radius fits in the spectroscopic aperture of the GAMA survey (angular radius = 1″). This is lower than the SDSS maximum mass due to narrower fiber aperture (SDSS fiber aperture is 1.5″). See Section 6.2 and Figure 10.

Those candidates identified through LinKS machine learning spanned a slightly higher redshift range and tended to be more massive, with the majority of candidates above $\log(M_*/M_\odot) \sim 11$. As Figure 11 shows, high scoring LinKS candidates can be found throughout the redshift-mass range, with the highest scoring around $\log(M_*/M_\odot)$ 11.5. This is because the training set for the Petrillo et al. (2018) LinKS machine learning method is based on intermediate redshift massive galaxies (LRGs) that would have been identified in SDSS spectroscopy, i.e. the SLACS identified sample.

GalaxyZoo identified candidates definitively below the catalog's $z < 0.15$ cutoff distributed in the mass range $\log(M_*/M_\odot) \sim 10.0 - 11.0$.

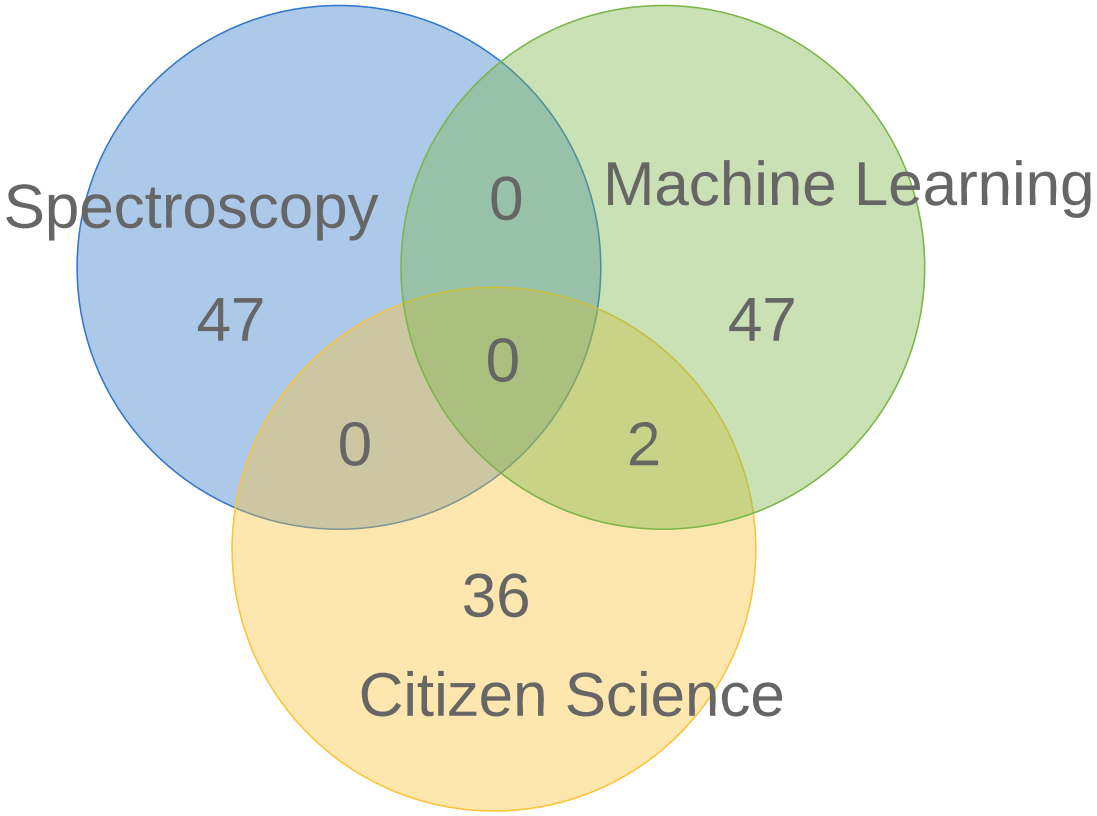

Figure 7. Venn diagram showing the number of lens candidates identified by each of the three methods following our final cuts. Overlapping regions indicate the number of lens candidates identified by both (or all three) candidates, while numbers in each methods' region indicate the total number of candidates identified by that method. The two overlaps occurred between 47 LinKS machine learning candidates and the 36 GalaxyZoo citizen science candidates.

Table 1. Overlap of LinKS Machine Learning and GalaxyZoo citizen science Samples.

GAMAID	RA	DEC	$(M_*/M_\odot)$	z	θ_E (arcsec)	ML Score	GZ Score
G136604	175.87	-1.74	2.87×10^{11}	0.106	2.63	58	31.65%
G124486	179.73	-2.52	8.54×10^{10}	0.144	1.24	28	42.62%

4.3. *Overlapping Candidates*

The two candidates (G136604 and G124486) common to both LinKS machine learning and GalaxyZoo citizen science, fall within the overlap of the parameter space occupied by the two methods' samples in terms of stellar mass and redshift, as shown in Figure 9. Their masses are (G136604) $2.87 \times 10^{11}(M_*/M_\odot)$ and (G124486) $8.54 \times 10^{10}(M_*/M_\odot)$ and redshifts z = 0.106 and z = 0.144. The "Lens or arc" score given to these candidates in GalaxyZoo citizen science (G136604: 31.65% and G124486: 42.62%) and the visual inspection scores from LinKS machine learning (G136604: 58 and G124486: 28) make these two of the most promising candidates.

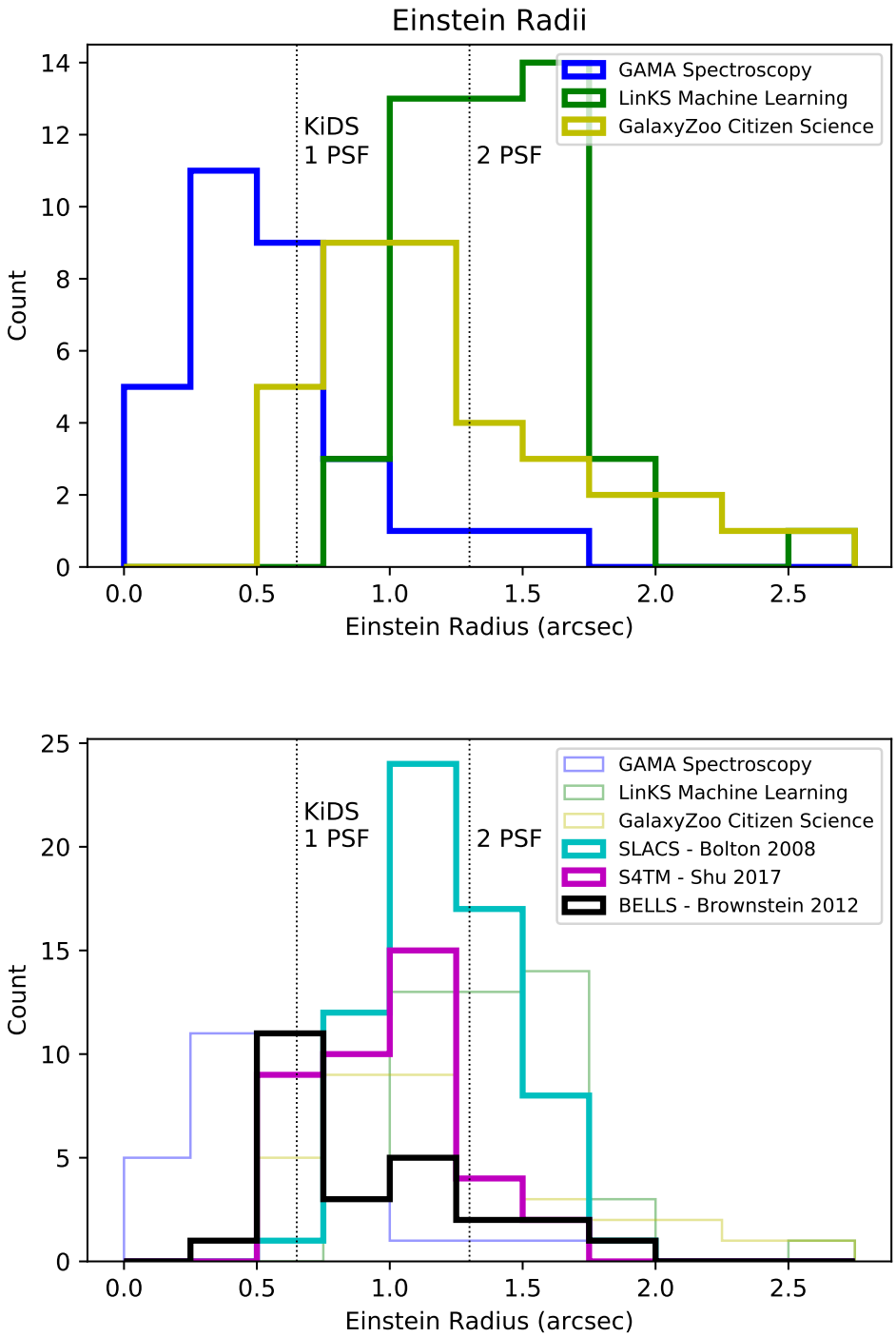

Figure 8. Einstein radius estimates for (upper) candidates of the three methods examined in this study and (lower) candidates identified by previous spectroscopic lens surveys. Section 3.3 details calculations for the three GAMA/KiDS methods, while estimates for SLACS, S4TM, and BELLS candidates are taken from Bolton et al. (2008a), Shu et al. (2017), and Brownstein et al. (2012).

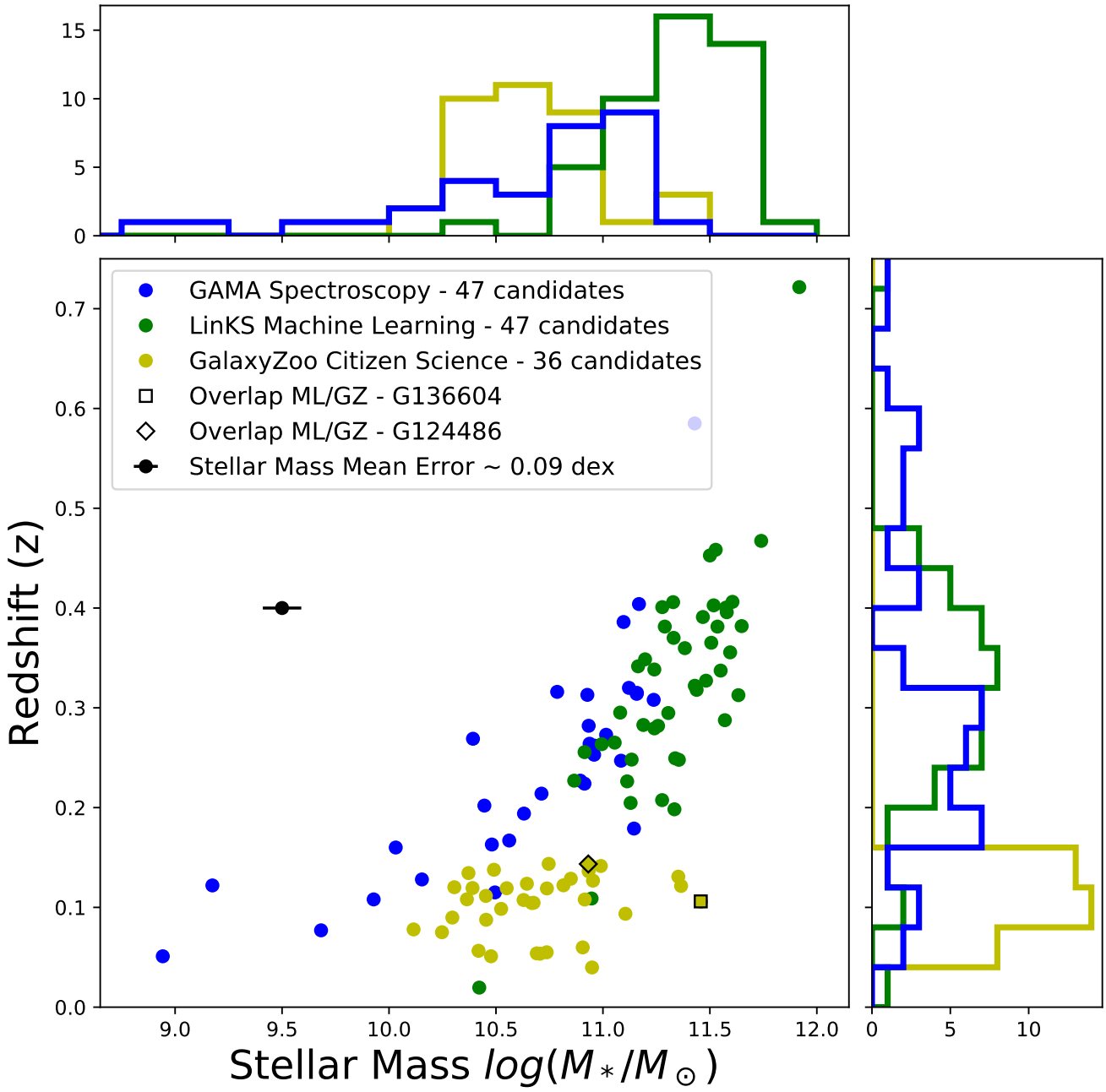

Figure 9. Distribution of lens candidates identified by each of the three methods in terms of each candidate's stellar mass and redshift. Histograms above and to the right of the scatter plot indicate the number of candidates identified by each method within specific ranges of stellar mass and redshift respectively. Each method's catalog occupies a unique range of both characteristics. The black marker with error bar represents mean uncertainty in stellar mass measurement to 1σ.

5. SELECTION EFFECTS

GAMA spectroscopy candidates are selected from a parent subsample of spectroscopic targets in the equatorial regions of GAMA DR3 with spectral template matches of greater than 90% confidence to one of three passive galaxy templates in the autoz algorithm. Stellar masses and redshifts are taken from the GAMA MAGPHYS catalog, and the resulting sample of passive galaxies in GAMA is taken to be the "parent sample" for comparison with the GAMA spectroscopy lens candidate sample. Kolmogrov-Smirnoff tests between the lens candidate sample and the passive

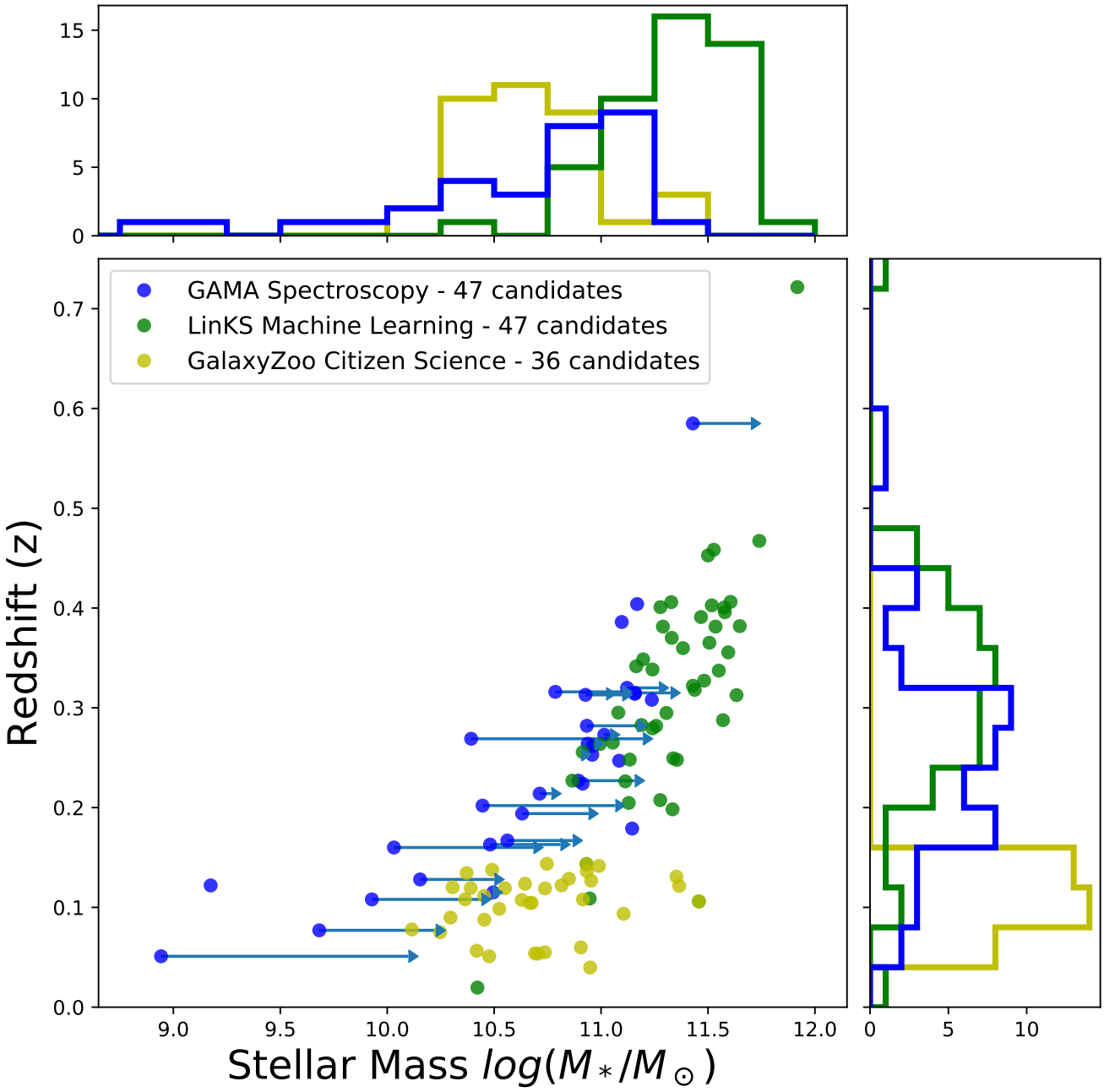

Figure 10. The data presented here is the same as in Figure 9 with additional error bars introduced to represent the estimated maximum stellar mass that could be enclosed by an Einstein radius of $\theta_E = 1$ arcsecond (corresponding to the aperture-size of GAMA spectroscopic fibers). Several candidates identified by the other two methods have mass that exceed this maximum mass at the given lens candidate redshift.

galaxy sample reveal K-S metrics and p-values of 0.0845 and 0.877 in terms of redshift and 0.340 and 2.433×10^{-5} in terms of stellar mass. This analysis is suggestive (but not significantly, with high p-value) of parity between the parent sample and candidate sample in terms of redshift. The high metric and low p-value for stellar mass indicate a difference between the samples, showing that GAMA spectroscopy does present bias in the mass range of identifiable candidates.

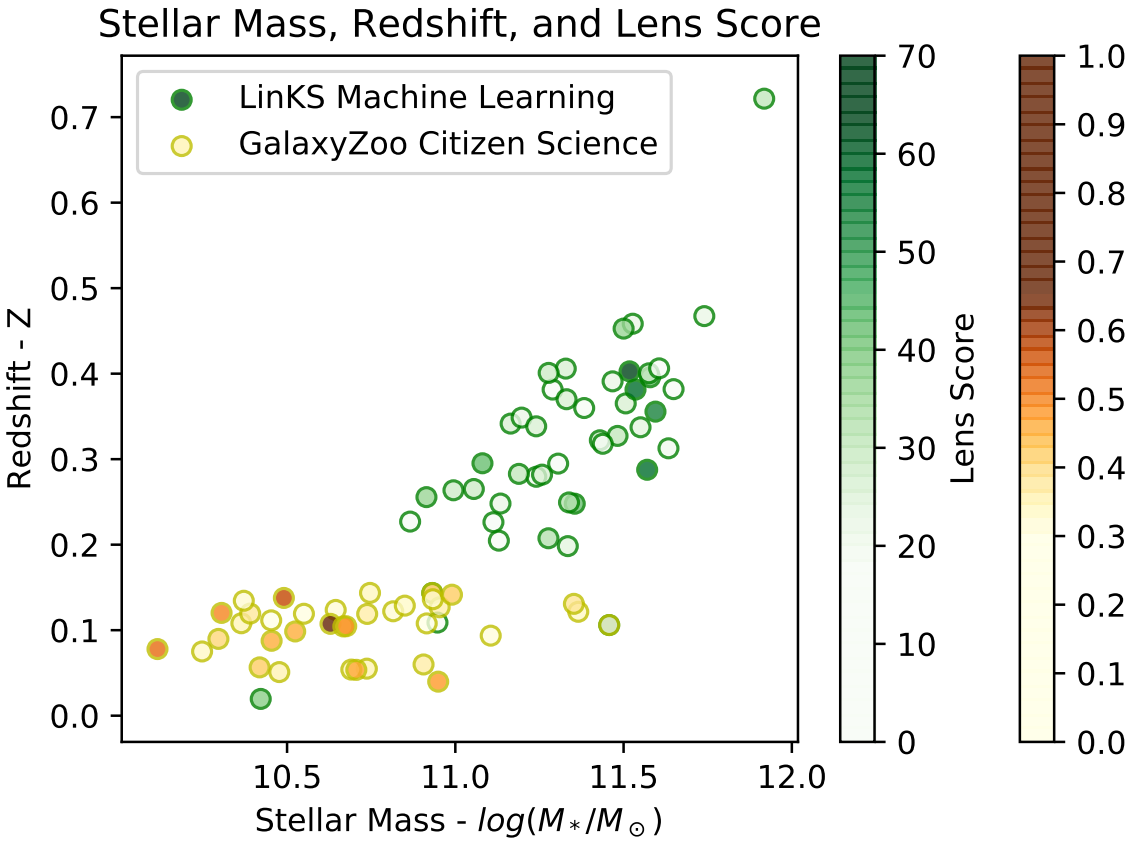

Figure 11. Green markers show the stellar mass and redshift of strong lens candidates identified by LinKS machine learning from (**?**). LinKS lens score reflected by the green color bar refers to the authors' visual inspection and scoring of candidates on a scale of 0-70, with higher numbers reflecting higher confidence. High-scoring objects occur throughout the mass and redshift range, with the highest scoring above $\log(M_*/M_\odot)$ 11.5. Yellow-to-brown markers indicate the stellar mass and redshift of our final selection of GalaxyZoo candidates (Kelvin et al *in prep*). GalaxyZoo lens score shown by the yellow-to-brown color bar refers to the fractional score out of 1 indicating the fraction of votes for "Lens or arc" for each candidate, with higher numbers reflecting higher confidence. High-scoring objects occur throughout the mass and redshift range.

The LinKS sample (**?**) of machine learning candidates, like its training sample, was selected using color-magnitude cuts modified from the SDSS-LRG (Large Red Galaxy) (Eisenstein et al. 2001; Petrillo et al. 2017; **?**) low-z selection criteria. The parent sample for candidates selected within the GAMA equatorial regions includes all galaxies within those regions that satisfy the LRG criteria. Color-magnitude selection includes the following:

$$r < 20$$

$$c_{perp} < 0.2$$

$$r < 14 + \frac{c_{par}}{0.3}$$

where

$$c_{par} = 0.7(g - r) + 1.2[(r - i) - 0.18)]$$

$$c_{perp} = (r - i) - \frac{g - r}{4.0} - 0.18$$

AB magnitudes are taken from GAMA Lambdar SDSS $g-$, $r-$, and $i-$ catalogs. Stellar mass and redshift are taken from GAMA MAGPHYS. K-S tests between the LinKS machine learning lens candidate sample and the GAMA equatorial LRG sample reveal (K-S metrics, p-values) of $(0.329, 5.23 \times 10^{-05})$ in terms of redshift and $(0.663, 4.57 \times$

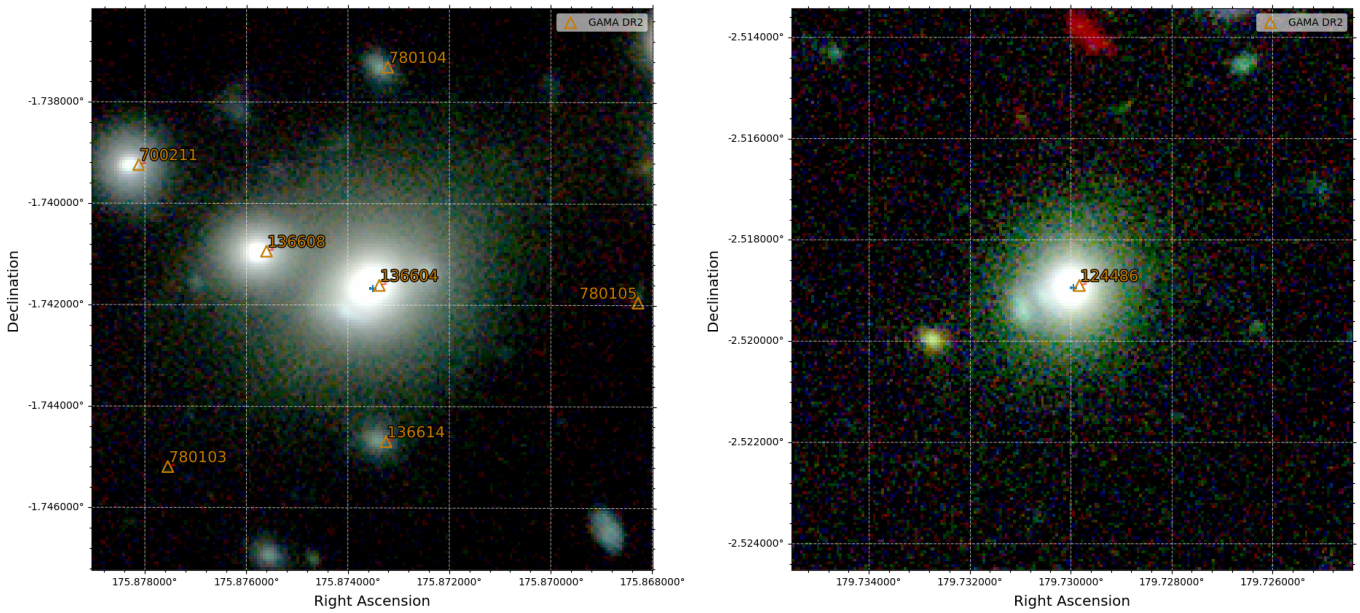

Figure 12. G136604 and G124486, the two candidates identified by both LinKS machine learning and GalaxyZoo citizen science. NOTE SCORES: score given to these candidates in GalaxyZoo citizen science (G136604: 31.6% and G124486: 42.6%) and the visual inspection scores from LinKS machine learning (G136604: 58 and G124486: 28).

10^{-19}) in terms of stellar mass. This demonstrates to high significance that the LinKS machine learning sample is not representative of its parent sample, as it it optimized for identifying high-mass candidates at low redshift.

GalaxyZoo selects only objects whose redshift $z < 0.15$, so the parent sample for the GalaxyZoo lens candidate sample contains all galaxies within the GAMA equatorial fields below that redshift upper limit. Redshifts and stellar masses are taken again from the GAMA MagPhys catalog, and K-S tests of redshift and stellar mass yield (K-S metric, p-value) of (0.0997, 0.849) and (0.621, 4.92×10^{-13}) respectively. This indicates a preference for high-mass candidates within its narrow redshift range.

Lensing searches of any kind prefer higher mass, with the exception of GAMA spectroscopy, which has an upper mass limit for identification at a given redshift due to its fixed aperture size (See Section 6.2 and Figure 10). GAMA spectroscopy and GalaxyZoo citizen science show no redshift bias from their respective parent sample due to the former's spectroscopic completeness and the latter's narrow redshift range. LinKS machine learning shows a combined redshift and mass difference between the candidate sample and the color-magnitude selected parent sample, indicating that the bias is instituted after the parent sample selection.

6. DISCUSSION

6.1. *LinKS machine Learning Training Set*

Machine learning is an effective method for identifying image features similar to the training set utilized. Its effectiveness is then constrained inherently by the scope of its training set. The catalog analyzed here from Petrillo et al. (2018) used simulated images resembling SLACS lenses as their training set, and the candidates it identified are characteristically similar in terms of Einstein radius, stellar mass, and redshift to those identified by SLACS spectroscopy. With a training sample volumetrically skewed towards massive elliptical galaxies (the early-type galaxies sample in KiDS) with large Einstein radii, the resulting identified candidates are equally biased toward higher masses and Einstein radii, as shown in Figures 8 and 13. This bias can be amplified through the problem of transfer learning.

6.2. *Maximum Stellar Mass in GAMA Spectroscopic Identification*

Lens candidate identification through any spectroscopic method requires sufficient flux from the background galaxy in order to obtain a second spectral match. For lensing systems whose Einstein radius exceeds the radius of the instrument's aperture, the probability of detection goes down significantly (Sonnenfeld et al. 2015, and reference therein). For lensing systems with known lens and source redshifts, there is then a soft constraint on the maximum

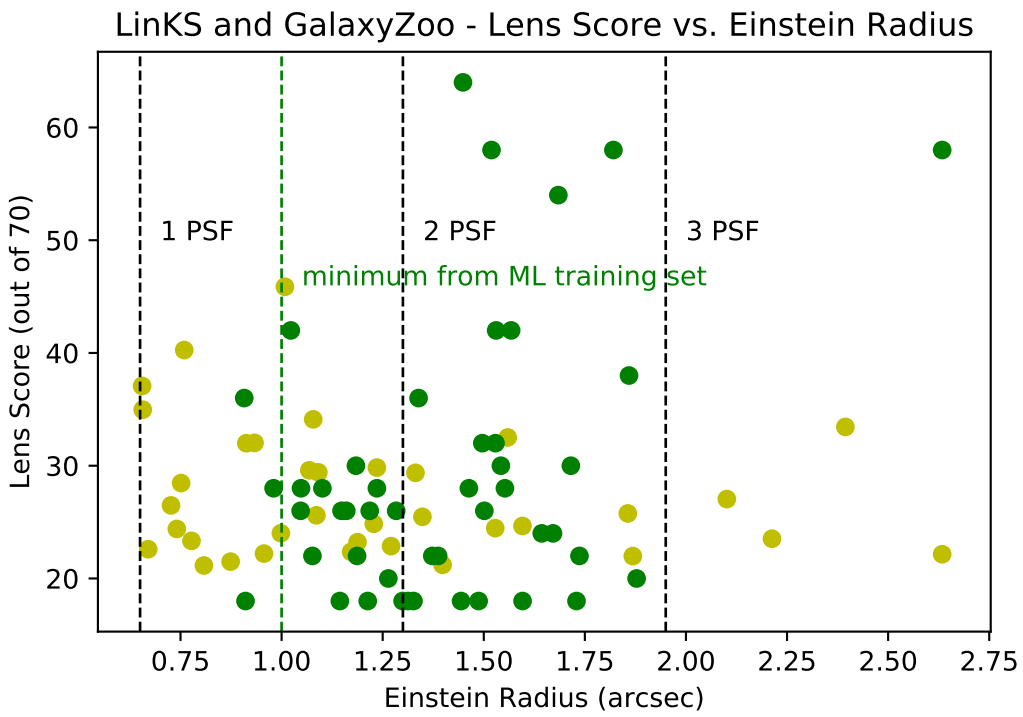

Figure 13. High scoring LinKS machine learning candidates show Einstein radii above the mininum $(1\prime\prime) utilized for the training set.$

total mass that will contribute to an Einstein radius that will fit within the instrument's aperture. Taking into account GAMA spectroscopy's 1″-radius aperture and assuming $f_{DM} = 61\%$, the estimates for this upper limit to stellar mass are calculated and shown as error-bars in Figure 10. Several candidates from the other two methods have stellar masses exceeding this upper limit at similar redshifts. This ensures that GAMA spectroscopy will have little chance of observing enough flux from the background galaxy to acquire the second redshift match required for candidate identification.

6.3. *Low-Mass Lensing Galaxies*

GalaxyZoo citizen science and GAMA spectroscopy found an encouraging number of candidates at lower masses than those identified through the LinKS machine learning method considered here, as well as most previous lens studies that focused on galaxies fitting the description of SDSS LRGs (Eisenstein et al. 2001). These candidates could potentially be analyzed in order to study the structure of galaxies and their dark matter content in this lower range of galaxy mass. However, each arc from GalaxyZoo will need to be confirmed spectroscopically before modeling these as lensing systems, and more samples are needed in order to study this parameter space with meaningful results.

6.4. *Candidates and LRG Color-Magnitude Selection*

The color-magnitude selection criteria for SDSS-LRGs detailed in Section 5 were applied to the final candidate samples of the LinKS machine learning and GalaxyZoo citizen science methods. Only 6 of the 36 GalaxyZoo candidates and 7 of the 47 LinKS candidates passed this selection, indicating that the more strong lenses are to be found by broadening the search and training sets beyond the assumption of LRG dominance, a result also found in (Li et al. 2020).

6.5. *Other Lens Searches and Future Efforts*

Similar efforts, mostly machine learning, have found strong lens candidates in deep imaging surveys (e.g., Speagle et al. 2019; Huang et al. 2019; Jacobs et al. 2019, in HSC, DECaLS and DES respectively). Figure 14 shows the GAMA equatorial lens candidates of this work and includes candidates previously identified by DECaLS, SLACS (Bolton et al.

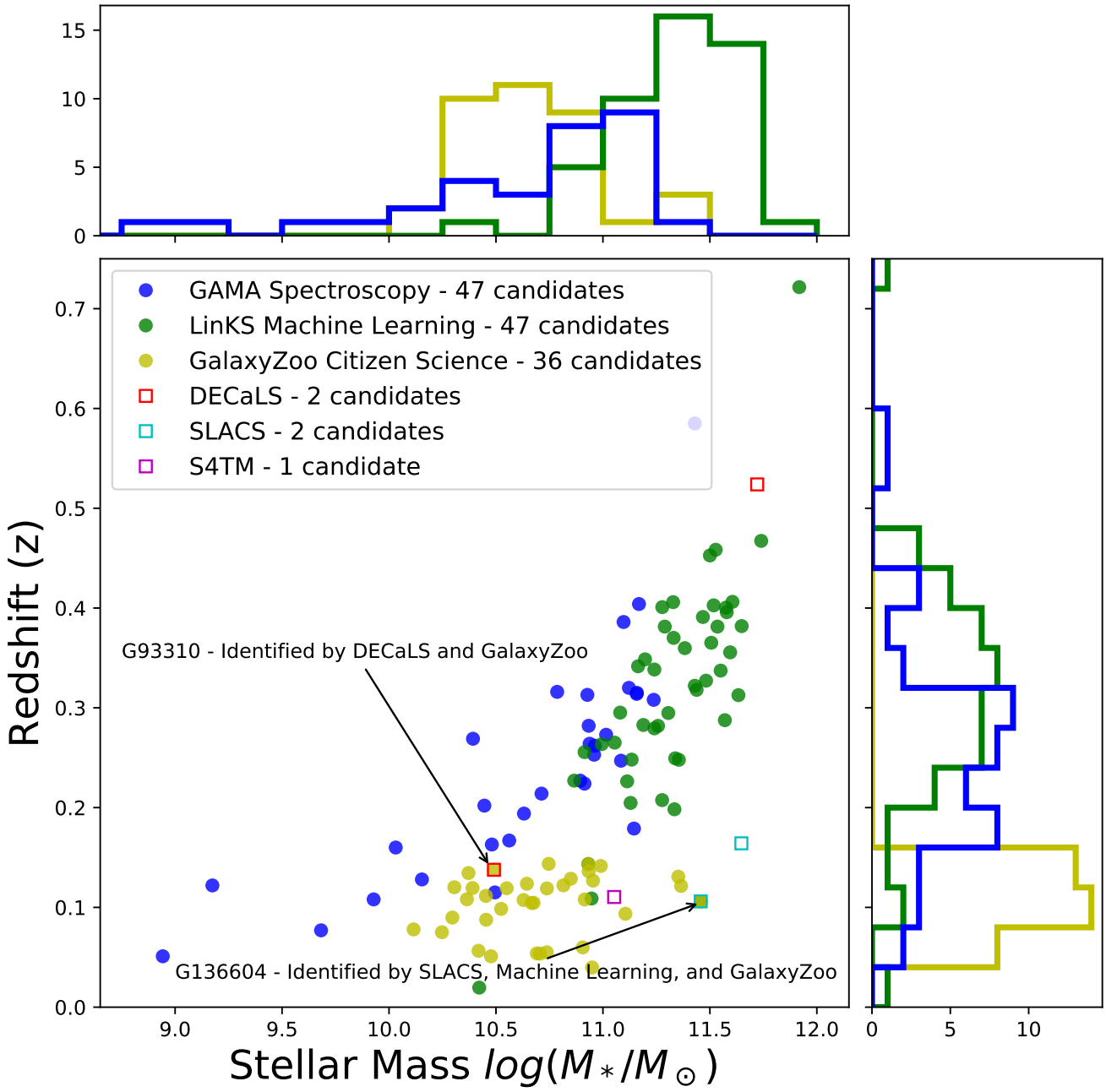

Figure 14. The data here is the same as in Figure 9 with the addition of five square markers indicating candidates previously identified by DECaLS (Huang et al. 2019), SLACS (Bolton et al. 2008a), and S4TM in the GAMA equatorial regions and which had a match in RA/DEC to the GAMA catalog. Two of these candidates were identified by GalaxyZoo citizen science, and one of those two was also identified by LinKS machine learning.

2008a), and S4TM (Shu et al. 2017) in the GAMA equatorial regions and which had a match in RA/DEC to the GAMA catalog. Two of these candidates were identified by GalaxyZoo citizen science, and one of those two was also identified by LinKS machine learning. This lends confidence to GalaxyZoo's ability to return high quality lens candidates. Figure 15 shows the numbers of identified lens candidates per unit of sky against the survey characteristics. The majority of theses studies aimed for a clean (reliable but incomplete) rather than complete sample of galaxy-galaxy lenses. Our results show that the combination of methods implies a much higher sky density of lenses in a given survey. Key for

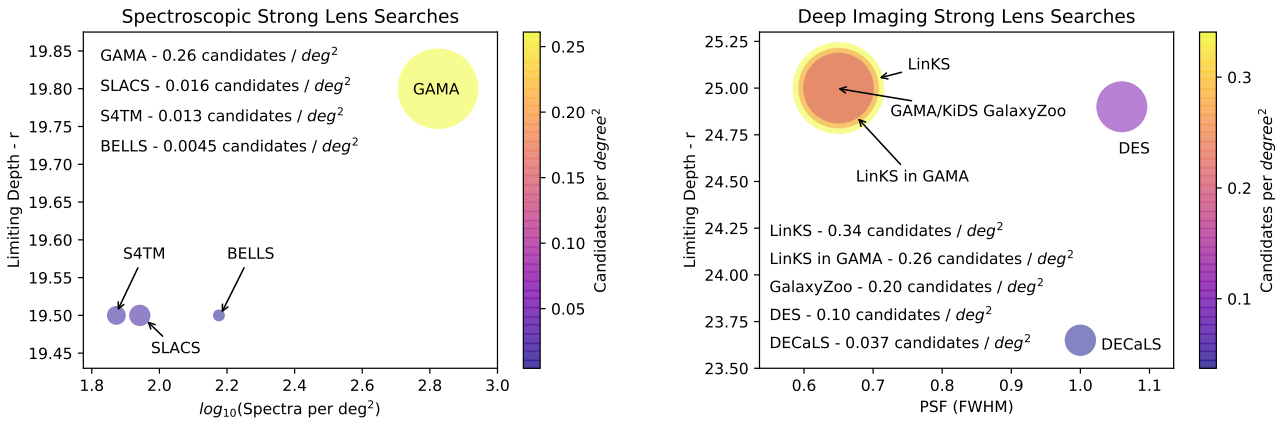

Figure 15. A comparison between the different identifications of strong galaxy-galaxy lens candidates in different surveys, using blended spectroscopy (left) and deep imaging (right). The left figure shows SLACS (Bolton et al. 2006), S4TM (Shu et al. 2017) and BELLS (Brownstein et al. 2012) spectroscopic searches compared to the GAMA spectroscopy candidates selected in this work from (Holwerda et al. 2015). The right figure shows the LinKS survey from **?** and the candidates presented in this paper from GAMA/KiDS GalaxyZoo citizen science, compared with deep imaging searches in DES (Jacobs et al. 2019) and DECaLS (Huang et al. 2019).

Table 2. Strong lenses with archival Hubble data available from the Hubble Legacy Archive.

GAMAID	RA	DEC	Method
G136604	175.87349	-1.74167	ML & GZ
G204703	139.07321	-0.40157	ML
G3882191	133.69397	-1.36032	ML
G593852	218.0782	-0.03958	GZ

spectroscopic survey identification is completeness, a key driver of GAMA survey (Driver et al. 2009; Robotham et al. 2010; Baldry et al. 2011), and an automated redshift finder (Baldry et al. 2014). For imaging surveys, the key drivers are spatial resolution (subarcsecond seeing) and survey depth. The on-sky density of strong lenses is critical if one wants to estimate, for example, the rates of strongly lensed events such as supernovae (Holwerda et al. *submitted*).

During the preparation of this paper, Li et al. (2020) published the results of their CNN's selection of strong lens candidates in the KiDS DR4 data using a technique similar, though slightly modified from the LinKS machine learning method. They offer qualitative comparison to Petrillo et al. (2018) and Petrillo et al. (2019), noting that their application of the CNN to an expanded sample of "bright galaxies" without LRG cuts doubled the number of quality lens candidates identified by their algorithm. Their result supports this work's assertion that the expansion of machine learning's scope beyond the standard assumption of LRGs will improve the completeness of such automated lens-finding methods. Li et al. (2020) further note their intention to follow with more quantitative comparison with the LinKS candidates in a future paper, as well as commenting on the value of comparison with other lens-finding methods. The follow-up study of that data in comparison with the data from this study is worth conducting.

The Hubble Legacy Archive (HLA) (Whitmore et al. 2016) contains imaging information on four of the lensing candidates presented here in Table 2. Figure 16 shows two of these examples. G136604 was identified in both the LinKS machine learning and GalaxyZoo citizen science selections (shown also in Figure 12, left) and was a known strong lens from the SLACS survey (Bolton et al. 2008b; Auger et al. 2010; Barnabè et al. 2011; Bolton et al. 2012; Czoske et al. 2012; Shu et al. 2015). The second example, G204703, is part of a cluster, and the arc is partially the result of cluster strong lensing (Zitrin & Broadhurst 2016; Zitrin 2017; Dessauges-Zavadsky et al. 2017; Newman et al. 2018). One of the GalaxyZoo identifications, G593852, is in the HLA, but the arc is faint in the Hubble single filter image (Figure 16). These images illustrate that all the selection methods find valid strong lens candidates and show that Hubble images on these would validate their nature and make detailed lensing models possible.

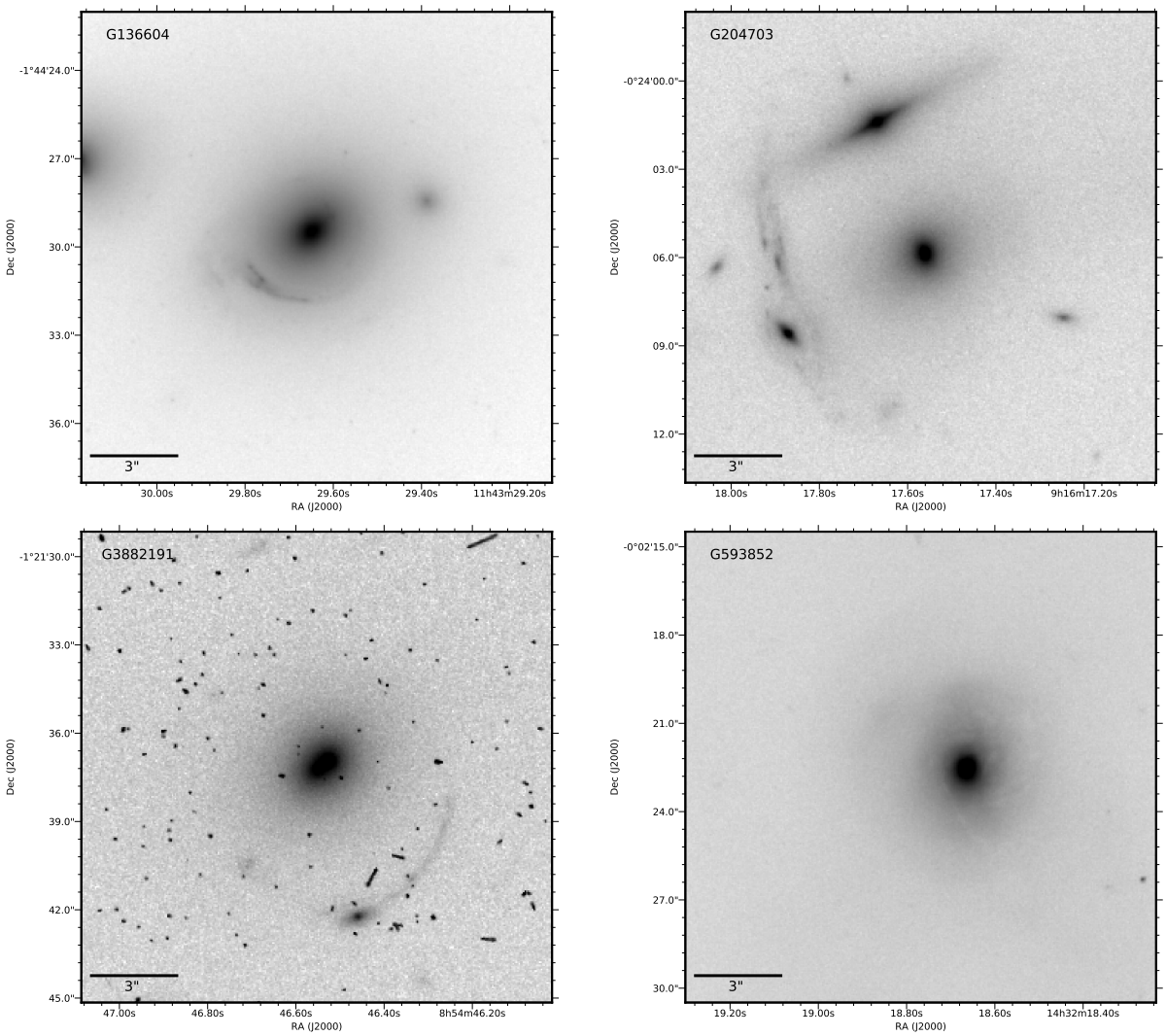

Figure 16. Examples of lensing candidates found in the Hubble Legacy Archive (HLA). Grayscale image in F814W, except G593852, which is in F625W. F625W is significantly narrower than F814W, which results in the lower contrast of the image of G593852. G136604 was identified earlier in SLACS, by LinKS machine learning and GalaxyZoo citizen science. The arc next to G204703 may be due to cluster lensing. G3882191 was identified in SLACS previously, and G3882191 is the faint arc identified by GalaxyZoo.

With improved spatial resolution for wide-field imaging (WFIRST and EUCLID), the machine learning and citizen science identification will overlap more in mass and redshift with the spectroscopic identifications of strong lens candidates. Wide-field integral field spectroscopy (e.g. SAMI, MUSE, and 4MOST WAVES wide surveys) could potentially identify strong lenses from a mix of spectroscopic and imaging information (curved arc in the data-cube). Future large telescopes (GMT/ELT/TMT) could follow-up the higher redshift or lower mass lens candidates, and the WEAVE and 4MOST instruments are set to select or confirm many candidates spectroscopically.

For future identification of galaxy-galaxy lenses (e.g. LSST or WFIRST imaging), a hybrid approach between citizen science and machine learning (see Beck et al. 2018) could result in a more complete and reliable yield of strong lensing candidates. This is in our view a better approach than to try to validate galaxy-galaxy lens candidates using different methods. A worthwhile next step will be to design and implement a CNN with a more complete training set using our findings and the work of Petrillo et al. (2019) and Li et al. (2020) to experiment with its application to KiDS imaging and HST archival data and to prepare for future wide-field imaging surveys. Figure 17 shows that several of the candidates unidentified by LinKS machine learning could be recovered in these deeper surveys that will be able to resolve the features of lenses with even the smallest of Einstein radii from this study. We believe the deliberate

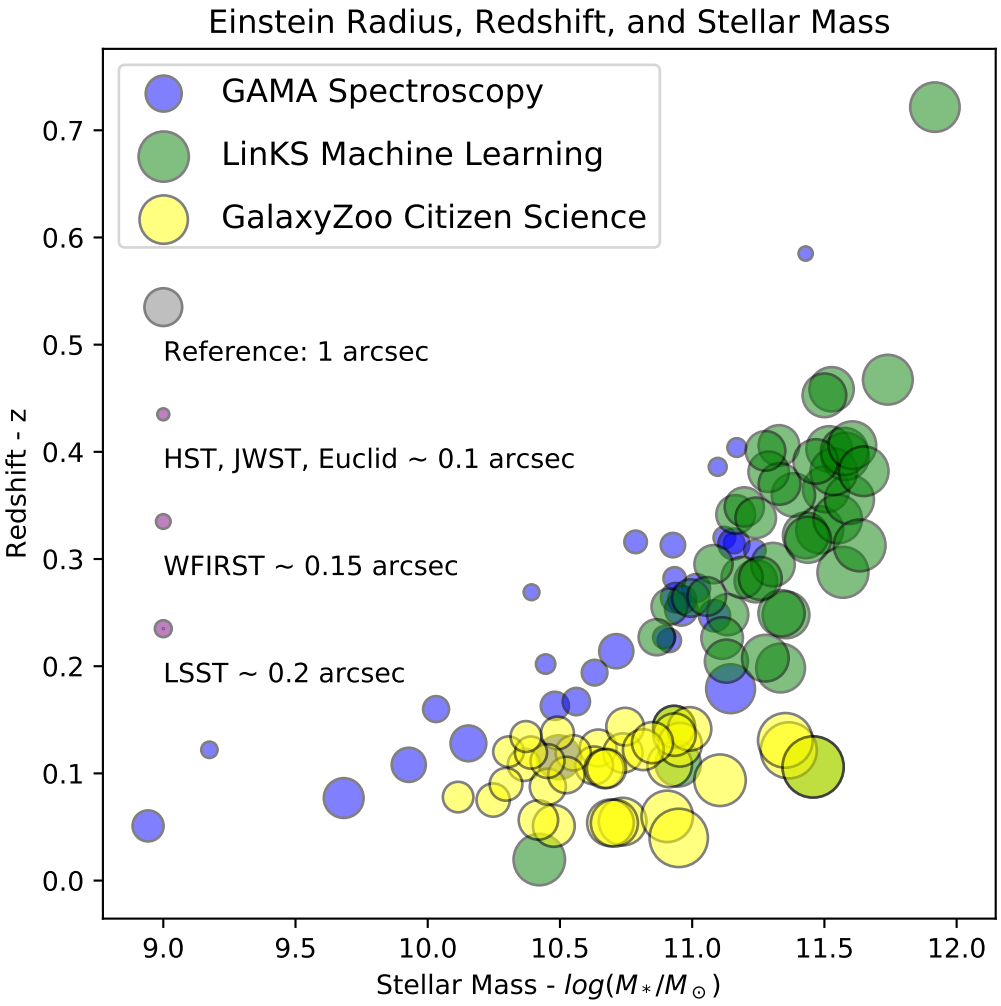

Figure 17. The data presented here is the same as in Figure 9 with marker-size corresponding to Einstein radius. The largest of Einstein radii tend to be at higher mass and lower redshift. The gray reference marker indicates the benchmark of $\theta_E = 1$ arcsecond (corresponding to the aperture-size of GAMA spectroscopic fibers). Next generation surveys (JWST, Euclid, WFIRST, LSST) will have optical resolutions comparable to HST, on the order of 0.1-0.2 arcseconds. In theory, under the right conditions, these surveys should be able to resolve even the smallest Einstein radii ($\theta_E = 0.141$ arcsec) considered in this survey.

expansion of the training set to include lenses with color features beyond the LRG assumption will improve the completeness a step further than that achieved by Li et al. (2020). Detection and modeling of these smaller lenses may reveal insights into dark matter fractions in the lower mass regime. Alternatively, an entirely new selection technique could result in a selection of similar completeness as the three presented here.

7. CONCLUSIONS

Our analysis of the data generated by the three methods leads us to the following conclusions regarding the biases and advantages of the methods as well as the relation of each to the others:

- The three specific methods analysed here are ineffective means of vetting candidate samples obtained by either of the other two methods due to the lack of overlap between candidate properties, which we illustrate in Figures 7 and 9.

- The differences in candidate properties arise primarily from selection functions inherent to the parent sample selections and procedures of each method; specifically:
  - Blended spectra identifies only those candidate galaxies whose lens features contribute significant flux within the radius of the fiber aperture collecting the spectrum. GAMA's depth and completeness extend candidate selection to a lower mass range. A wider aperture or integral field spectroscopy (e.g. SAMI or MUSE) would allow the possibility of identifying lower redshift or more massive galaxies.
  - Machine learning finds candidates with similar features to its training sets, i.e. well-separated lens and arc. This limitation can be improved upon with higher-resolution images and a wider variation in training sets, including lens galaxies that do not conform to LRG characteristics.
  - GalaxyZoo's upper threshold on redshift limits its range of applicability, and the wide focus of its classification stage introduces significant challenges to candidate quality assessment. Higher-resolution images and a higher redshift cutoff together would allow for the inclusion of farther galaxies, e.g. for WFIRST, LSST, or Euclid citizen science efforts.
- Machine learning has the promise to be the most efficient automated lens identification technique, and substantial effort must be made to improve these algorithms ahead of the next generation of galaxy surveys.
- In the meantime, other methods – including blended spectra and citizen science – remain useful for extending and diversifying the catalog of lens candidates available for study and for their application in the training of machine learning algorithms.

Strong gravitational lenses offer a unique laboratory to be used in cosmology measures and the next level of accuracy in estimates of dark matter distribution and substructure. The much greater samples needed (orders of magnitude higher than the current number of identified lenses) require automated identification. Using a combined systematic approach to improve the scope of machine learning's applicability, a more complete census of these rare objects can be achieved for the next generation of imaging surveys (e.g. WFIRST, Euclid, and LSST).

ACKNOWLEDGEMENTS

S. Knabel acknowledges the support of the Summer Research Opportunity Program (SROP) and the Undergraduate Research Grant (URG) by the University of Louisville's Office of the Executive Vice President for Research and Innovation (EVPRI). The material is based upon work supported by NASA Kentucky under NASA award No: NNX15AR69H (R. Steele).

8. APPENDIX

Table 3. GalaxyZoo Citizen Science Lens Candidates

GAMA ID	Lens Score	$\log(M_*/M_\odot)$	z	$\theta_E(arcsec)$	RA (deg)	DEC (deg)
511867	35.22%	10.74	0.055	1.596	216.39	-1.11
485873	34.95%	10.69	0.054	1.528	217.75	-1.80
70022	36.81%	10.91	0.060	1.856	178.02	0.07
170898	33.61%	11.37	0.122	2.213	176.47	-2.34
184275	31.73%	10.64	0.124	0.956	175.92	-1.44
84050	36.58%	10.74	0.119	1.086	175.80	0.48
7104	33.33%	10.25	0.075	0.777	175.71	0.83
55245	31.41%	11.11	0.094	1.869	181.08	-0.32
70282	65.54%	10.63	0.107	1.008	179.40	0.13
185451	30.30%	10.91	0.108	1.398	180.28	-1.61
124486	42.62%	10.93	0.144	1.236	179.73	-2.52
106562	36.39%	10.95	0.127	1.348	216.63	0.84
593852	38.63%	11.35	0.131	2.101	218.08	-0.04
593691	34.84%	10.36	0.108	0.741	217.51	-0.12

Table 3. GalaxyZoo Citizen Science Lens Candidates

GAMA ID	Lens Score	$\log(M_*/M_\odot)$	z	$\theta_E(arcsec)$	RA (deg)	DEC (deg)
568545	35.50%	10.48	0.051	1.228	215.50	-0.59
460645	30.71%	10.55	0.119	0.874	213.23	-1.72
93803	47.77%	10.95	0.040	2.394	222.49	0.56
93310	57.51%	10.49	0.138	0.759	219.92	0.51
136604	31.65%	11.46	0.106	2.634	175.87	-1.74
600421	42.02%	10.42	0.057	1.091	135.49	0.28
574423	46.43%	10.71	0.054	1.559	135.76	-0.20
324764	42.28%	10.67	0.104	1.069	137.20	1.73
218733	41.96%	10.99	0.142	1.331	140.30	0.89
320551	52.96%	10.11	0.078	0.655	218.68	1.78
342699	45.71%	10.45	0.088	0.913	216.90	2.13
363319	45.75%	10.52	0.099	0.933	218.85	2.57
418788	34.31%	10.75	0.144	0.998	137.69	2.75
422113	49.96%	10.31	0.120	0.657	129.42	2.60
422228	30.21%	10.45	0.112	0.808	129.94	2.59
196837	48.73%	10.68	0.105	1.078	132.91	-0.70
372045	37.83%	10.39	0.119	0.727	133.97	0.98
3632594	32.67%	10.93	0.136	1.271	138.25	-0.96
3578853	31.95%	10.82	0.122	1.172	130.98	-1.62
287627	32.28%	10.37	0.134	0.670	174.20	1.69
164403	40.66%	10.30	0.090	0.752	177.42	-2.73
238271	33.17%	10.85	0.129	1.188	213.73	1.58

8.1. *Alternate Cuts*

The final cuts were intended to ensure a comparable and reliable catalog of lens candidates for each method analyzed. The numbers reflected in our final catalogs will vary if considered under different cuts, so we also examined the overlap considering a more relaxed cut that included all GAMA spectroscopy candidates, all LinKS machine learning candidates with scores greater than 0, and all GalaxyZoo candidates with lens scores greater than 20%. Figure 18 shows that this cut improves overlap to a small extent, but it introduces a significant increase in false-positives and unreliable candidates, which we considered to outweigh the benefits of the improvement to overlap for the purposes of this study. The overlaps that we see in the more relaxed cuts do appear in the expected parameter space, with masses and redshifts comparable to the two overlap candidates that appear in our final catalogs.

REFERENCES

Arneson, R. A., Brownstein, J. R., & Bolton, A. S. 2012, ApJ, 753, 4

Auger, M. W., Treu, T., Bolton, A. S., et al. 2009a, ApJ, 705, 1099

—. 2009b, ApJ, 705, 1099

—. 2010, ApJ, 724, 511

Baldry, I. K., Driver, S. P., Loveday, J., et al. 2011, ArXiv e-prints

Baldry, I. K., Alpaslan, M., Bauer, A. E., et al. 2014, MNRAS, 441, 2440

Baldry, I. K., Liske, J., Brown, M. J. I., et al. 2018, MNRAS, 474, 3875

Barnabè, M., Czoske, O., Koopmans, L. V. E., Treu, T., & Bolton, A. S. 2011, MNRAS, 415, 2215

Beck, M. R., Scarlata, C., Fortson, L. F., et al. 2018, ArXiv e-prints

Bolton, A. S., Burles, S., Koopmans, L. V. E., et al. 2008a, ApJ, 682, 964

Bolton, A. S., Burles, S., Koopmans, L. V. E., Treu, T., & Moustakas, L. A. 2006, ApJ, 638, 703

Bolton, A. S., Burles, S., Schlegel, D. J., Eisenstein, D. J., & Brinkmann, J. 2004, AJ, 127, 1860

Bolton, A. S., Treu, T., Koopmans, L. V. E., et al. 2008b, ApJ, 684, 248

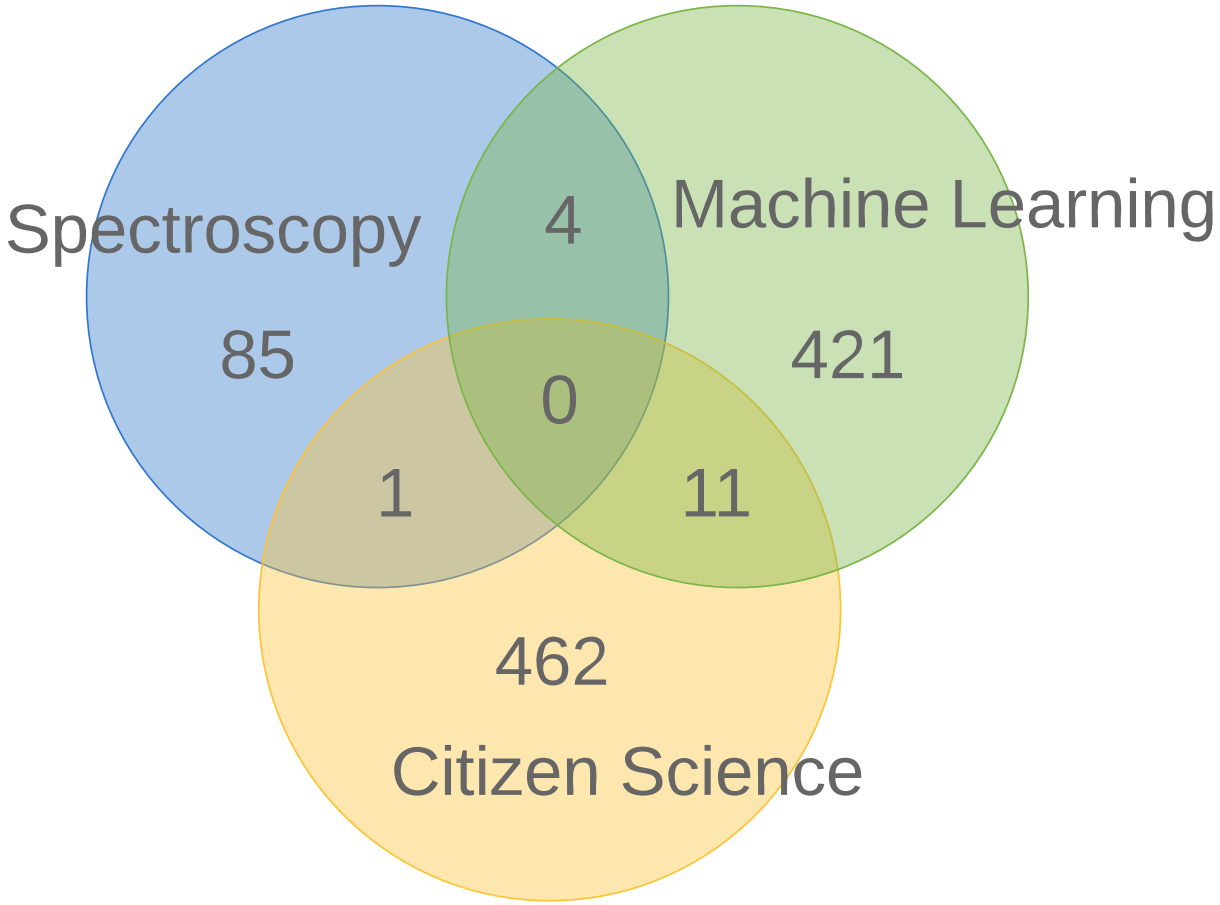

Figure 18. Venn diagram showing the number of lens candidates identified by each of the three methods with more lenient cuts to both GalaxyZoo citizen science and LinKS machine learning. Candidates with "Lens or arc" scores above 20% and LinKS machine learning candidates with lens scores greater than 0 are included in this selection. Overlapping regions indicate the number of lens candidates identified by both (or all three) candidates.

Bolton, A. S., Schlegel, D. J., Aubourg, E., et al. 2012, ArXiv e-prints

Brownstein, J. R., Bolton, A. S., Schlegel, D. J., et al. 2012, ApJ, 744, 41

Chan, J. H. H., Suyu, S. H., More, A., et al. 2016, ApJ, 832, 135

Chen, G. C.-F., Fassnacht, C. D., Suyu, S. H., et al. 2019, MNRAS

Cluver, M. E., Jarrett, T. H., Hopkins, A. M., et al. 2014, ApJ, 782, 90

Collett, T. E., Oldham, L. J., Smith, R. J., et al. 2018, ArXiv e-prints

Collier, W. P., Smith, R. J., & Lucey, J. R. 2018a, MNRAS, 473, 1103

—. 2018b, ArXiv e-prints

Cyr-Racine, F.-Y., Keeton, C. R., & Moustakas, L. A. 2018, ArXiv e-prints

Czoske, O., Barnabè, M., Koopmans, L. V. E., Treu, T., & Bolton, A. S. 2012, MNRAS, 419, 656

de Jong, J. T. A., Verdoes Kleijn, G. A., Kuijken, K. H., & Valentijn, E. A. 2013, Experimental Astronomy, 35, 25

de Jong, J. T. A., Verdoes Kleijn, G. A., Boxhoorn, D. R., et al. 2015, A&A, 582, A62

de Jong, J. T. A., Kleijn, G. A. V., Erben, T., et al. 2017, A&A, 604, A134

De Lucia, G., Springel, V., White, S. D. M., Croton, D., & Kauffmann, G. 2006, MNRAS, 366, 499

Dessauges-Zavadsky, M., Zamojski, M., Rujopakarn, W., et al. 2017, A&A, 605, A81

Driver, S. P., Norberg, P., Baldry, I. K., et al. 2009, Astronomy and Geophysics, 50, 050000
Driver, S. P., Hill, D. T., Kelvin, L. S., et al. 2011, MNRAS, 413, 971
Eisenstein, D. J., Annis, J., Gunn, J. E., et al. 2001, AJ, 122, 2267
Gavazzi, R., Treu, T., Koopmans, L. V. E., et al. 2008, ApJ, 677, 1046
Gavazzi, R., Treu, T., Rhodes, J. D., et al. 2007, ApJ, 667, 176
Hilbert, S., White, S. D. M., Hartlap, J., & Schneider, P. 2008, MNRAS, 386, 1845
Holwerda, B. W., Baldry, I. K., Alpaslan, M., et al. 2015, MNRAS, 449, 4277
Holwerda, B. W., Kelvin, L., Baldry, I., et al. 2019, AJ, 158, 103
Hopkins, A. M. 2018, ArXiv e-prints
Huang, X., Domingo, M., Pilon, A., et al. 2019, arXiv e-prints
Jacobs, C., Collett, T., Glazebrook, K., et al. 2019, arXiv e-prints
Koopmans, L. V. E., Treu, T., Bolton, A. S., Burles, S., & Moustakas, L. A. 2006, ApJ, 649, 599
Kuijken, K., Heymans, C., Dvornik, A., et al. 2019, arXiv e-prints
Li, J., Jia, S., Gao, Y., et al. 2020, arXiv e-prints, arXiv:2004.14587
Lintott, C. J., Schawinski, K., Slosar, A., et al. 2008, MNRAS, 389, 1179
Liske, J., Baldry, I. K., Driver, S. P., et al. 2015, MNRAS, 452, 2087
Newman, A. B., Belli, S., Ellis, R. S., & Patel, S. G. 2018, ApJ, 862, 125
Petrillo, C. E., Tortora, C., Chatterjee, S., et al. 2017, MNRAS, 472, 1129
—. 2018
Petrillo, C. E., Tortora, C., Vernardos, G., et al. 2019, MNRAS, 484, 3879
Riess, A. G., Macri, L., Casertano, S., et al. 2011, ApJ, 730, 119
Robotham, A., Driver, S. P., Norberg, P., et al. 2010, PASA, 27, 76
Shu, Y., Bolton, A. S., Brownstein, J. R., et al. 2014, ArXiv e-prints
—. 2015, ApJ, 803, 71
Shu, Y., Brownstein, J. R., Bolton, A. S., et al. 2017
Sonnenfeld, A., Treu, T., Marshall, P. J., et al. 2015, ApJ, 800, 94
Speagle, J. S., Leauthaud, A., Huang, S., et al. 2019, arXiv e-prints
Tortora, C., Koopmans, L. V. E., & Napolitano, N. R. 2017, ArXiv e-prints
Treu, T., Gavazzi, R., Gorecki, A., et al. 2009, ApJ, 690, 670
Treu, T., Koopmans, L. V., Bolton, A. S., Burles, S., & Moustakas, L. A. 2006, ApJ, 640, 662
Verlinde, E. P. 2016, ArXiv e-prints
Whitmore, B. C., Allam, S. S., Budavari, T., et al. 2016, ArXiv e-prints
Wright, A. H., Driver, S. P., & Robotham, A. S. G. 2018, MNRAS
Zitrin, A. 2017, ApJ, 834, 45
Zitrin, A., & Broadhurst, T. 2016, ApJ, 833, 25